Study of High Speed Impact on Composite Armor Structure

Author

Muhammad Muzamil

Regn Number

00000275930

Supervisor

Dr. Aamir Mubashar

DEPARTMENT OF MECHANICAL ENGINEERING

SCHOOL OF MECHANICAL & MANUFACTURING ENGINEERING

NATIONAL UNIVERSITY OF SCIENCES AND TECHNOLOGY

ISLAMABAD

November 2021

Study of High Speed Impact on Composite Armor Structure

Author

Muhammad Muzamil

Regn Number

00000275930

A thesis submitted in partial fulfillment of the requirements for the degree of

MS Mechanical Engineering

Thesis Supervisor:

Dr. Aamir Mubashar

Thesis Supervisor's Signature: _____

DEPARTMENT OF MECHANICAL ENGINEERING

SCHOOL OF MECHANICAL & MANUFACTURING ENGINEERING

NATIONAL UNIVERSITY OF SCIENCES AND TECHNOLOGY,

ISLAMABAD

November 2021

Declaration

I certify that this research work titled "**Study of High Speed Impact on Composite Armor Structure**" is my own work. The work has not been presented elsewhere for assessment. The material that has been used from other sources it has been properly acknowledged / referred.

Signature of Student

Muhammad Muzamil

2018-NUST-MS-Mech-00000275930

Thesis Acceptance Certificate

Certified that final copy of MS thesis written by **Mr. Muhammad Muzamil** Registration Number No. **275930** of SMME has been verified by undersigned, found complete in all respects as per NUST States/Regulations, is free of plagiarism, errors, and mistakes and is accepted as partial fulfilment for the award of MS degree. Is further certified that necessary amendment as pointed out by GEC members of the scholar have also been incorporated in the said thesis.

Signature: _____

Name of Supervisor: Dr. Aamir Mubashar

Signature (HOD): _____

Date: _____

Signature (Principal): _____

Date: _____

Certificate for Plagiarism

It is certified that MS Thesis Titled: **"Study of High Speed Impact on Composite Armor Structure",** by **Muhammad Muzamil (Reg.275930)** has been examined by me. I undertake the follows:

a. Thesis has significant new work/knowledge as compared already published or are under consideration to be published elsewhere. No sentence, equation, diagram, table, paragraph, or section has been copied verbatim from previous work unless it is placed under quotation marks and duly referenced.
b. The work presented is original and own work of the author (i.e., there is no plagiarism). No ideas, processes, results, or words of others have been presented as Author own work.
c. There is no fabrication of data or results which have been compiled/analyzed.
d. There is no falsification by manipulating research materials, equipment, or processes, or changing or omitting data or results such that the research is not accurately represented in the research record.
e. The thesis has been checked using TURNITIN (copy of originality report attached) and found within limits as per HEC plagiarism Policy and instructions issued from time to time.

Name & Signature of Supervisor

Dr. Aamir Mubashar

Signature**:** _____

Plagiarism Certificate (Turnitin Report)

This thesis has been checked for Plagiarism. Turnitin report endorsed by Supervisor is attached.

Signature of Student

ABC

Registration Number

Signature of Supervisor

Copyright Statement

- Copyright in text of this thesis rests with the student author. Copies (by any process) either in full, or of extracts, may be made only in accordance with instructions given by the author and lodged in the Library of NUST School of Mechanical & Manufacturing Engineering (SMME). Details may be obtained by the Librarian. This page must form part of any such copies made. Further copies (by any process) may not be made without the permission (in writing) of the author.
- The ownership of any intellectual property rights which may be described in this thesis is vested in NUST School of Mechanical & Manufacturing Engineering, subject to any prior agreement to the contrary, and may not be made available for use by third parties without the written permission of the SMME, which will prescribe the terms and conditions of any such agreement.
- Further information on the conditions under which disclosures and exploitation may take place is available from the Library of NUST School of Mechanical & Manufacturing Engineering, Islamabad.

Acknowledgements

I am thankful to my Creator Allah Subhana-Watala to have guided me throughout this work at every step and for every new thought which you setup in my mind to improve it. Indeed, I could have done nothing without Your priceless help and guidance. Whosoever helped me throughout the course of my thesis, whether my parents or any other individual was Your will, so indeed none be worthy of praise but You.

I am profusely thankful to my beloved parents who raised me when I was not capable of walking and continued to support me throughout in every department of my life.

I would also like to express special thanks to my supervisor, Dr. Aamir Mubashir for his help throughout my thesis and for guiding me selflessly in whole time. Each time I got stuck in something, he came up with the professional help. Without his help I wouldn't have been able to complete my thesis. I appreciate his patience and guidance throughout the whole thesis.

I would also like to thank Dr. Emad uddin, Dr. Zaib Ali, and Dr. Najam Ul Qadir for being on my thesis guidance and evaluation committee. I am also thankful to Mr. Haseeb Ahmed and Mr. Manzar Masood for their continues support and cooperation.

Finally, I would like to express my gratitude my parents and all the individuals who have rendered valuable assistance to my study.

Dedicated to my exceptional parents and adored siblings whose tremendous support and cooperation led me to this wonderful accomplishment

Abstract

In this research, a numerical investigation is reported in finding out the ballistic limit velocities of various sandwich structures when subjected to high speed impact. Composite Armor structures consisting of Thermoplastic Polyurethane core and Aluminum AA 5083 – H116 face-sheets were studied to find out their ballistic limit velocities, perforation and penetration resistance. The dynamic response of the sandwich structures was investigated using finite element analysis package ABAQUS/EXPLICIT. The geometrical nonlinearities were considered for both the materials. The Aluminum face-sheets were modelled using Johnson-Cook's Material model while the TPU foam core was modelled using Ductile damage with Damage evolution model. Aluminum AA5083-H116 face skins were used as face skins with TPU cores of varying thicknesses to enhance the impact penetration and perforation resistance of sandwich structures. Increasing the thickness of face sheets and Core served to increase the impact and damage resistance. Increasing the thickness of face sheets from 1.2 mm to 1.5 mm and 2 mm thicknesses can enhance the ballistic resistance of structure up to 11.7% and 18.2%, respectively. By increasing the core thickness from 20 mm to 30 mm and 50 mm , ballistic resistance can be enhanced up to 30.6% and 40.8%, respectively. Target configuration, material parameters, projectile nose shape and impact velocity are some of the key factors that influence the ballistic response of the structure. The numerical methodology is found to be more efficient and reliable in the prediction of ballistic limit velocities and damage resistance of composite armor structures with more accurate results and this surely can replace the time consuming and expensive dynamic experiments**.**

Key words: High speed Impact, Composite sandwich structures, Ballistic simulation, Thermoplastic Polyurethane, Impact resistance, Abaqus FEA

Table of Contents

Table of Figures

CHAPTER 01: INTRODUCTION

Impact penetration and perforation resistance of different structures have been studied for long time, and numerous works have been done in order to understand the phenomena of impact events. Several factors effect the penetration and perforation processes in structural impact events. Several studies have been carried out to study and improve the response of engineering structures to high speed impact.

1.1. Background, Scope and Motivation

Sandwich structures, also known as foam cored sandwich structures, are engineering structures that consists of two thin and strong face sheets separated by light weight foam core. Increase in the moment of inertia due to separation of face skins by the core tends to improves its capability to withstand bending and buckling loads [1]. Numerous research studies have been carried out in the past on the design and development of sandwich panels that can endure high intensity impulsive loads [2–7]. The face sheets are generally Aluminum or fiber re-inforced polymers whereas the core is usually, wood, metal foams, polymers and metal honey combs. The behavior of sandwich structures either static or dynamic, have been studied extensively [8–9]. These structures are extensively used in both aerospace and naval structures due to their energy absorption capabilities, structural efficiency and durability.

In the recent studies, sandwich structures when subject to projectile impact, have offered great dissipation of impact energy as compared to monolithic armor plates with equal aerial density [10–12]. In another research study, it was found that monolithic plates offers more resistance to impact penetration due to increased bending resistance [13]. We may conclude from these research studies that the impact penetration and perforation resistance of sandwich panels, as compared to other designs, is dependent on certain impact situations.

In previous studies, core material and its density have been proven to be key factors and the selection of the proper material can optimize the performance of the structure. Both experimental as well as accurate numerical techniques are required to understand the material response and to improve the optimization process. AP Projectiles can easily penetrate through the armor plates. This phenomenon is difficult to understand using analytical relations. These analytical relations can only be applied under certain conditions[14]. In comparison, Experimental techniques can be

used to understand the impact event and materials' response with the help of high speed cameras and X-ray images. Borvik et al[15] conducted the analytical and experimental study to understand the behavior of Al 5083-H116 behavior with ogival nose shaped rods and 7.62 mm APM2 Projectiles. Residual velocity data and ballistic limit velocities were also calculated for armor plates.

Excessive deformation, erosion, high strain rate dependent nonlinear material behavior, and fragmentation are among problems associated with high speed impact and penetration. Modelling of penetration is carried out with all the aforementioned aspects in check. The penetration pattern and complex deformation that take place during ballistic impact, can now be easily computed using numerical methods and other various computer technologies. After a thorough study of the literature, it can be deduced that the majority of the attention is on the development and practical use of continuous hydro-codes [16]–[19]. Ls-Dyna, a well-known explicit code, has been successfully utilized to simulate a variety of armors subjected to impact for various danger levels and capable of using multiple simulation techniques [20]–[25].

Finite Element methods can accurately anticipate the material behavior of metallic armors as well as the underlying physics of bullet penetration [26]–[29]. To accurately anticipate material behavior under impact, Finite Element Simulation requires accurate material models. The flow stress of metallic plates is often modelled using the Johnson Cook's model, which predicts strain rate and temperature dependent material response. In order to properly characterize the material behavior, the Johnson-Cook material model requires the definition of a number of material properties.

Kilic & Namik [30] carried out numerical simulations on Secure 500 armox steel in which the ballistic limit thickness of secure 500 armour steel was computed using Lagrangian and smoothed particle hydrodynamics. The simulation is carried out using the SPH method, which is a particle-based model of continuum partial differential equations. The particles are not connected by edges as they are in a normal finite element mesh. Johnson Cook's and Johnson Cook's failure model are being used to record the behavior of the steel armor's material. To simulate the hydrodynamic behavior of a material, the Mie-Gruneisen equation of state is utilized. The steel armor plate was simulated utilizing an element erosion criterion, which brought mesh dependency into play. Element erosion increases when the mesh density of the Lagrangian finite element model is

increased. The findings obtained experimentally and numerically were found to be highly correlated with each other. Tria and Trebi [31] built a finite element model of a 7.62 mm AP bullet hitting 30 PM armor steel using a modified version of Johnson Cook's material model.

Polymers are commonly utilized as a sandwich structure's core material because of their low density and high energy absorption capabilities. Thermo- plastic polyurethane, a versatile polymer material in the family of polymers materials, exhibits highly ductile behavior and shows good stress strain recovery under both tension and compression. Jamil et al [32], [33] showed that when the impact energy increases, the energy absorption capability of TPU improves. TPU can with stand high impulsive loads and have the capacity to recover after being subjected to extreme loading conditions.

1.2. Goals and Motivation

To understand the response to impact loading a detailed study of the impact and penetration mechanics is required. Therefore a comprehensive relevant background and literature survey is of prime importance to carry out this research precisely. The major objective of this research is to use finite element analysis to investigate the behavior of composite sandwich structure under high-speed impact. The main objectives of this research are,

- To analyze the response of sandwich structures when impacted with ogival shaped nose Armor piercing projectiles.
- To analyze the plastic deformation and its concentration in sandwich structures during impact.
- To analyze the behavior of sandwich structures of different core sizes upon impact.
- To determine the effect of hole pattern in core and face sheets on ballistic resistance of structure.
- To determine the potential benefits and ballistic limits of sandwich structures of different thicknesses.
- To evaluate the failure mechanism occurred on sandwich structures upon high speed impact.
- To analyze and compare variable approaches to determine the failure criterion.
- To validate the FEA simulation models of ballistic impacts on sandwich structures by employing the data available in literature.

1.3. Research Methodology

For improvement and optimization of shielded armors, and before executing their accreditation, one could use the predictive ability of Finite Element codes to save cost involved in experimentation. Since such numerical analysis (huge deformations and fragmentation) is an extensive and separate research field for the CAE-branch, therefore some of the base is needed. A solution to deal with initial computational ballistics model depends on detailed literature study. The methodology of the current research based on some of the relevant fields of study are shown in the form of a chart in the **Figure 1**,

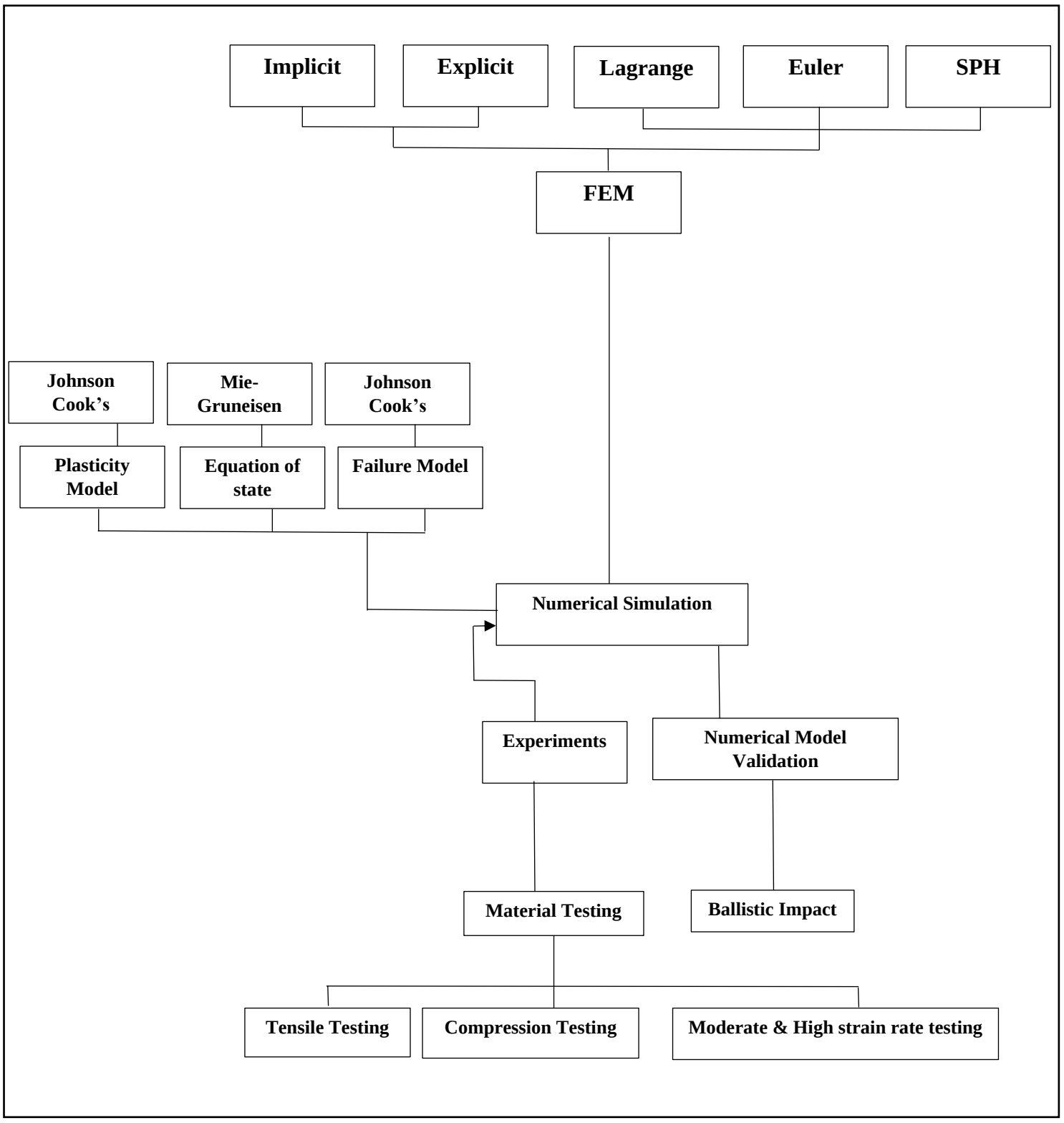

Figure 1: Research Methodology

2. CHAPTER 02: LITERATURE REVIEW

In high-tech applications such as aircraft, spacecrafts, race cars and naval ships, innovative and high-performance load-bearing part design is often pursued. These structures should be light weight while maintaining a high strength-to-weight ratio. Structural efficiency can be achieved by properly selecting the most efficient material and an optimized structural design.

In addition to general stiffness and strength requirements, there can be other requirements on a structure. Fire protection, sound insulation, and impact protection requirements Thus, it is not always required to design a lightweight structure which meet general stiffness and strength requirements.

Various standards ought to be considered while choosing materials to be used in armor systems. There is not a single material which is considered as ideal. One material providing an adequate protection against one threat, can be dangerous to use to protect from other threats. Commonly used armor materials are as follow,

- ***Steel*** Homogenized rolled steel is tough, hard and powerful enough to stop the high speed impact and fast moving projectiles. It does not shatter once hit by high speed projectile.
- ***Aluminum*** is also widely used in protective structures to its less weight and high toughness properties. Normally, it is being used in APCs (armored personnel carrier) and armor cars.
- ***Plastic armors*** are widely used as they can stop the APPs Armor Piercing Projectiles by deflecting from their original trajectory and stuck between the plastic armor and base steel/Aluminum backing plate.
- ***Projectile Proof Glass*** is widely used in defense industry as it is immune to penetration when hit by a projectile.
- ***Ceramics*** are one of the most widely used for armor applications. Some notable ceramic materials are Tungsten Carbide, Silicon Carbide, Titanium Dibromide, Aluminum Oxide, Boron Carbide, and Aluminum Nitride.
- ***Composite material*** is a broader category of materials that can be used for armor protection and similar goals. Three main categories of composites are, Reinforced particle composites, Reinforced fiber composites and composite structures. This classification is illustrated as follow in **Figure *2***.

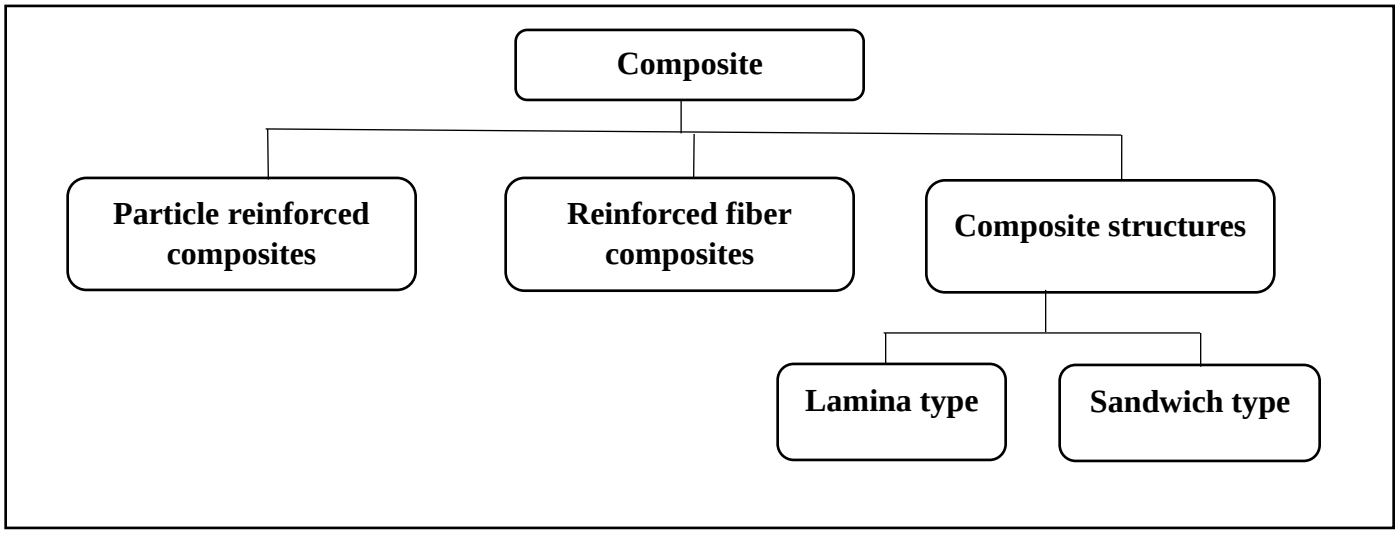

Figure 2: Classification of composites

2.1. Deformation in Metal Armors

When a metal or a material is subjected to a load, it deforms in an elastic and partly plastic manner. The deformation depends upon the type of material, applied force and the geometry of material. When a material is subjected to high speed impact, the internally generated heat due to friction and plastic deformation get no time to disperse away which results in massive local temperature rise, thermal softening and extensive plastic deformation or even failure. **Figure *3*** portrays an engineering stress-strain graph for a typical ductile material, which addresses different material behaviors when subjected to force/load.

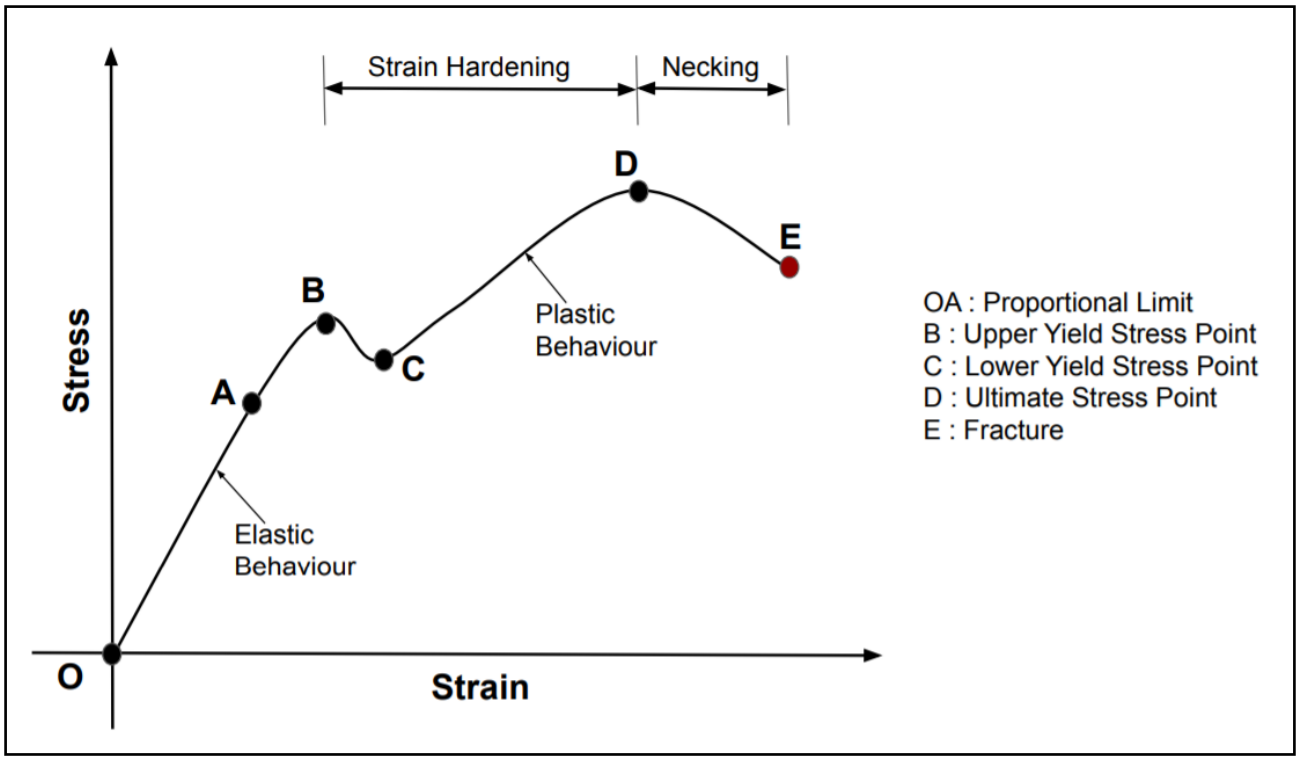

Figure 3: Stress strain graph for deformation in ductile materials [34]

2.1.1. Elastic Deformation

Elasticity is the ability of the material body to resist the deformation and return to its original size and shape when the applied load is removed. Elastic deformation can be expressed with the help of Hooke's law. Hooke's law is only applicable for material that deform linearly in their elastic region.

$$\boldsymbol{\sigma = E.\varepsilon} \qquad (1)$$

Where $\boldsymbol{E}$ represents the modulus of elasticity, $\boldsymbol{e}$ denotes the strain induced and $\boldsymbol{\sigma}$ represents the stress caused due to applied load. When the material reaches its yield point, its elastic deformation limits exceeds and material starts deforming plastically.

2.1.2. Plastic Deformation

When a material reaches to its yield point, a non-recoverable permanent plastic deformation occurs. In this zone, stress is no longer proportional to strain, and Hooke's law no longer applies.

The strength of a material to endure plastic deformation until rupture point defines whether the material is ductile or brittle. In ductile materials, elastic behavior, yielding, plastic deformation and necking are involved in deformation process. While, brittle materials have very less or low yielding behavior and may fracture upon very little plastic deformation without prior warning or notice.

The percentage elongation or the percentage area reduction until fracture in case of ductile materials can be expressed as:

$$\boldsymbol{Percentage\ elongation} = (\boldsymbol{lf} - \boldsymbol{lo}/\ \boldsymbol{l_f}) \times \mathbf{100}$$

$$\boldsymbol{Percentage\ area\ reduction} = (\boldsymbol{Ao} - \boldsymbol{Af}/\ \boldsymbol{Ao}) \times \mathbf{100}$$

Where lo is the initial or pre load length, lf is the length at fracture. Ao is the initial or pre load cross sectional area and Af represents the cross sectional area when material ruptures.

2.1.3. Deformation energy and fracture

When a material is distorted by an external loading, it tends to store strain energy with in it throughout its volume. Strain energy density is a parameter that is defined as the strain energy stored in a unit volume, it is expressed as,

$$u = \int \sigma \, d\varepsilon f \qquad (2)$$

Where, ε_f is the strain at rupture.

2.1.4. Modulus of Resilience

Modulus of resilience can be defined as " Elastic energy stored in a unit volume of a material without undergoing any plastic or permanent deformation". Modulus of resilience is also

known as elastic strain energy density. The elastic strain energy density is represented by the area under the stress-strain curve before the yielding point.

$$ur = \frac{1}{2} . \sigma 2/E2 \quad (3)$$

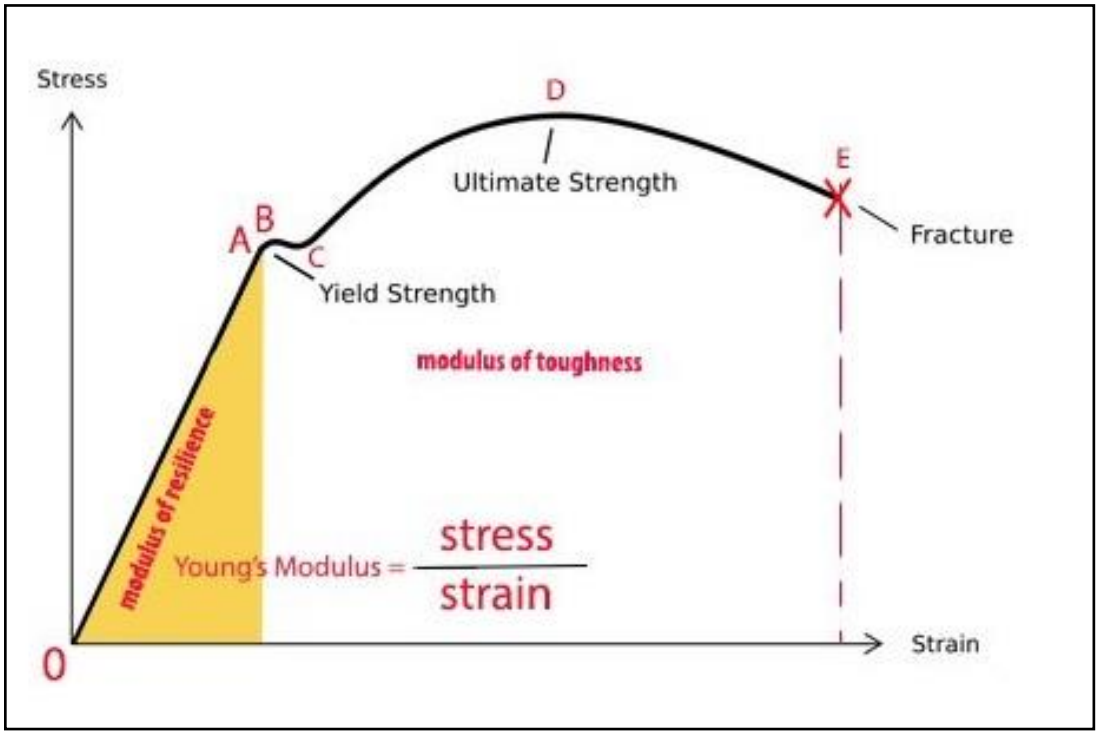

Figure 4: Modulus of Resilience [35]

2.1.5. Modulus of Toughness

Material's ability to absorb elastic and plastic strain energy till fracture point". This parameter is also known as strain-energy density of material. The area enclosed by the stress-strain graph until fracture point represents the modulus of toughness.

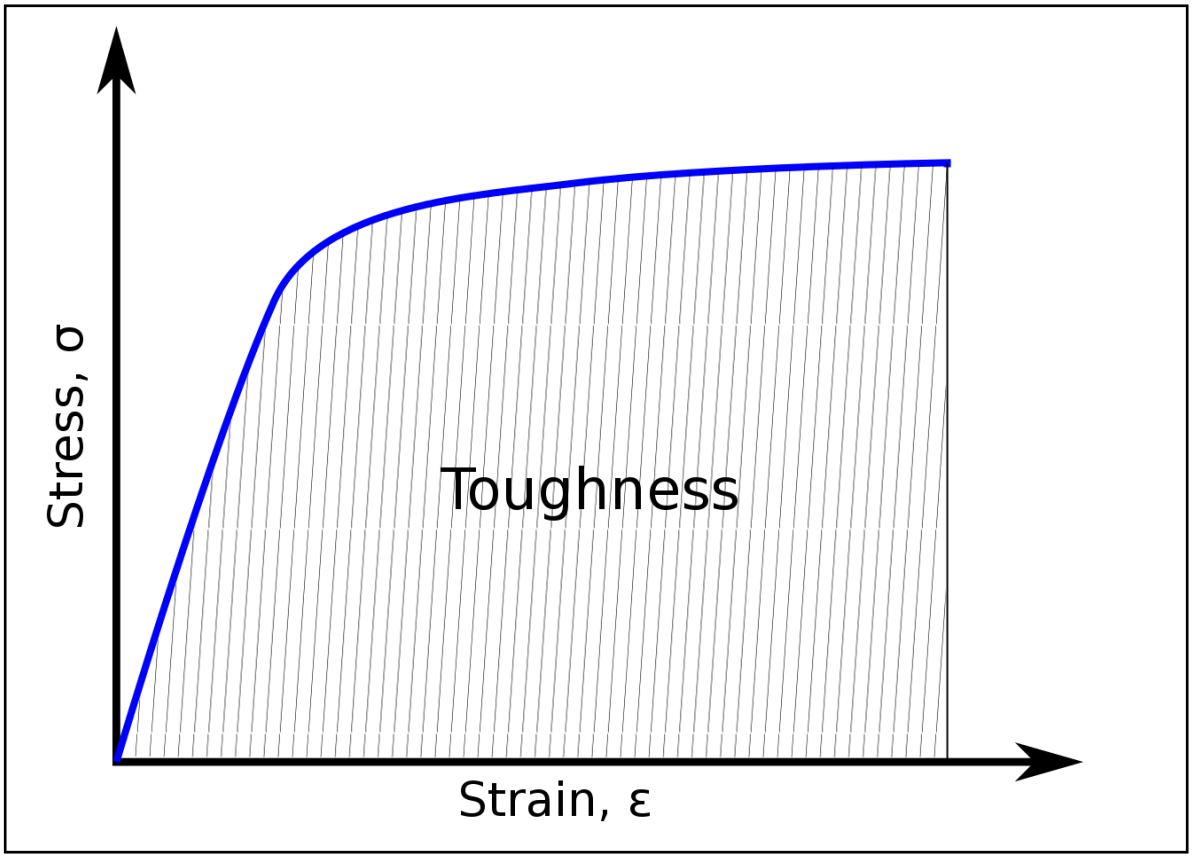

Figure 5 : Modulus of toughness

2.2. Deformation at high strain rate

Strain rate is the deformation rate of the material when an external force is applied on it. In comparison to low temperature deformations, time dependent deformation mechanisms vary more greatly at high temperatures. If the strain rate increases, The deformation process changes the material's temperatures to completely adiabatic. At high strain rate, the heat due to adiabatic heating does not have significant available time so the generated heat escapes out of material body upon deformation. This will cause an adiabatic shear instability, which will have a significant impact on the material's mechanical behavior. As deformation continues, adiabatic heating will occur in a very small area, causing the thermal softening of the material. As a consequence, adiabatic shear bands are formed on the material. Adiabatic shear bands (ASB) are thin regions of excessively deformed material due high strain rate loading which results in complete failure of material in many cases. ASBs are generally produced due to shock wave loading in material. Shock wave loading can be defined as the loading at high strain rates.

2.2.1. Adiabatic shear band

Adiabatic shear bands are the localized zones of intense shear which occurs when the material is deformed at high strain rate. At high strain rates, the internally generated heat in a material due to deformation has no time to disperse away from the material. As a result, the regions where contact loads occurs, experience shear loading and behave adiabatically. This leads to intense local temperature rise and thermal softening which results in extensive plastic loading or even complete failure of material. This phenomenon is known as adiabatic shear localization which makes the adiabatic shear bands. The localization of ASBs depends upon the velocity of the impact. With the present Finite element modelling technique, it is realistically impossible to capture the shear band formation phenomenon due to very small mesh size which results in excessive distortion of elements at high speed impact.

2.3. Failure mechanism in impact loading

When a high force or a shock is applied on a material for a very short interval of time, it is considered as Impact loading. The severity of impact load depends upon the weight and velocity of the impactor. When a projectile hits the body, its kinetic energy transfers to the targeted body and get converted into strain energy from kinetic energy. This transfer of energy deforms the armor material and deformation depends upon the impacting projectile energy and their contact velocity. If the deformation energy exceeds the enduring ability of the armor then the projectile will perforate through the armor material resulting in complete failure or damage. **Figure *6*** shows the various failure mechanisms of armors.

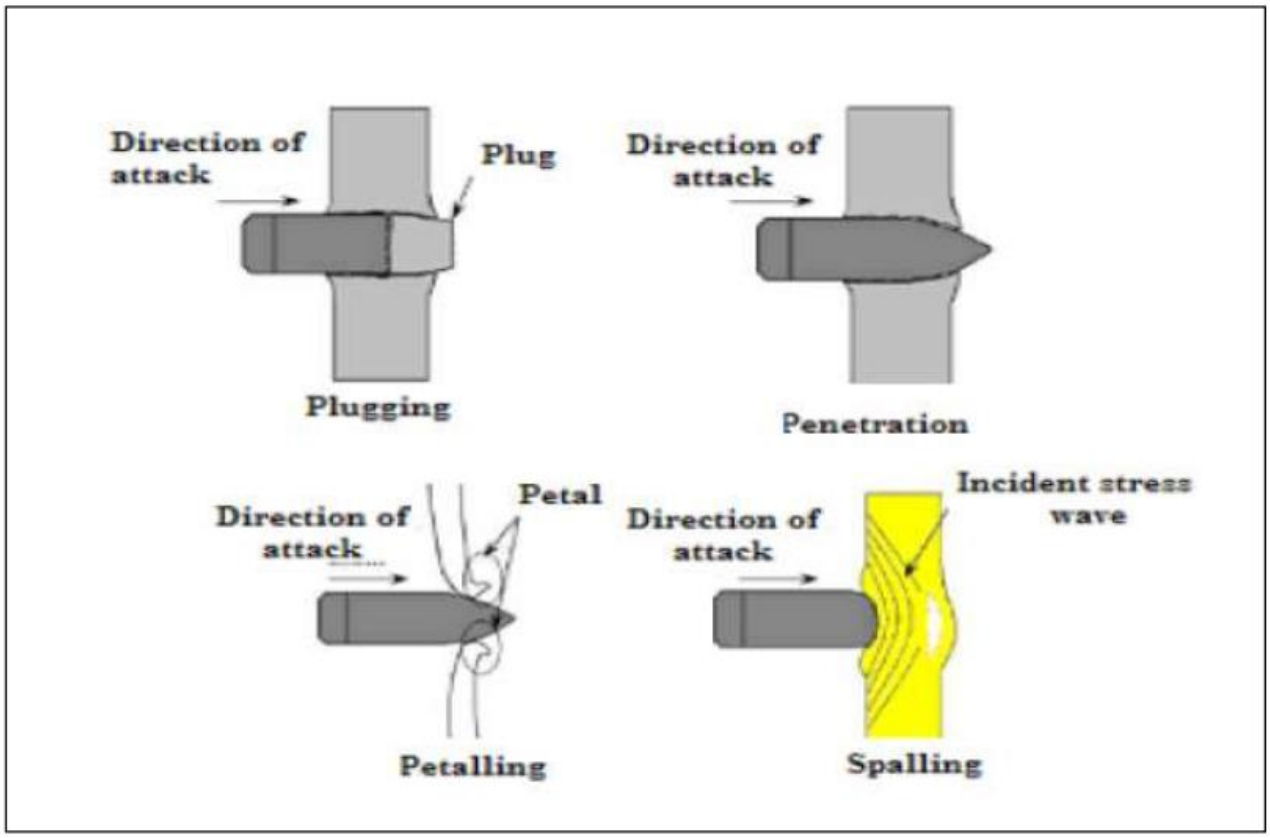

Figure 6: Failure mechanisms in impact loading [36]

Plugging is the material failure mechanism which occurs when the blunt or hemispherical nosed projectile with a very high velocity impacts the armor material close to ballistic limit of the material thus causing slugging in armor of roughly identical diameter as the projectile.

Penetration is the material failure mechanism which occurs when the projectile excavates into the target body beyond the thickness of spall crater. Penetration depth is the measure of cross section of the crater depth.

Petalling is the material failure mechanism in which the armor fails from the flow of the initial waves of stress due to excessive circumferential and radial tensile stresses. The maximum stress occurs close to the projectile tip. The projectile forward motion pushes the material in its direction of motion thus producing a bending stress in the armor plate thus causing the characteristic failure pattern. It is often determined in thin plates affected by cone-shaped projectiles at comparatively low velocities of impact near the ballistic limit.

Spalling is tensile failure mechanism in which the armor fails as a result of reflected impulse wave from the rear surface of armor plate by the impact of projectile. Spalling takes place in materials that are more vigorous in compression than they are in tension.

2.4. Numerical models for Ballistic Impacts

In previous years, a great advancement has been achieved in the field of research by the use of numerical modelling techniques to analyze different problem effectively and efficiently. In recent years, different numerical techniques have been used by various researchers to analyze the response of high strain rate of different materials under impact loading. Variety of numerical methods are being used by the researchers to get a realistic picture of high speed impact phenomenon. These methods are accurate as well as inexpensive as they save huge experimental cost involved in impact problems.

As discussed earlier, there are several methods available to understand the various stages of impact process. The most effective and realistic method is the experimental method but it involves extensive experience and huge experimental cost to conduct those experiments. Another, but most competitive and realistic approach is computer based numerical simulations to study the impact phenomenon. Numerical simulations provide accurate and detailed understanding of the impact and failure mechanisms of armors. Improved and optimized armor designs can also be achieved by using computer based numerical techniques as this method provides complex analysis and saves huge experimental cost and time.

Extensive research has already been performed to effectively model the impact loading mechanism and to demonstrate the damage and failure criteria of armor plates both at low and high velocities. Børvik et al.[37] effectively demonstrated the damage in ductile materials such as Weldox 460E steel using the explicit analysis technique of LS-DYNA software, they found that the computational numerical model is highly sensitive to mesh size and material defining parameters.

Nazeer et al. [38] used the mathematical model to successfully demonstrate the perforation and fracture mechanism of ductile metal targets when impacted by conical impactor, they found out that a numerical method can be used to effectively analyze the toughness of ductile armor sheets before fracture occurs during impact event. They also found out that, Rigid-plastic fracture mechanism can be used for mathematical and numerical analysis of toughness of ductile armor

sheets. Also, this analysis technique can be utilized to determine the number of cracks/petals formed when the material fractures.

Rusinek et al. [39] studied the damage evolution in mild steel sheets both numerically and experimentally. The impacted the mild steel plates with hemispherical nose shaped projectile and demonstrated the petal formation in ductile targets. They found out that the dislocation of petals in numerical simulation is quite similar to experimental results. To determine the ballistic limit thickness of Secure 500 armor steel, Ekici and Kilis [25] used numerical simulations utilizing the Lagrangian and SPH methods. The simulations are carried out using the SPH method, which is a particle-based model of continuum partial differential equations. Particles are not connected by edges like in a normal finite element mesh. The failure model being utilized is Johnson-Cook's plasticity which records the response of the steel armor's material. Modeling of hydrodynamic material response employs the Mie-Gruneisen equation of state. The steel armor plate was simulated utilizing an element erosion criterion, which brought mesh dependency into play. As the mesh density of Lagrange finite element models increased, which resulted in an increase in element erosion. The results of the experiments and the numerical results were found to be substantially linked. Tria and Trebi [31] built a finite element model of a 7.62 mm AP bullet hitting 30 PM armor steel using a modified version of the Johnson Cook's material model..

Borvik et al. [15] conducted the analytical and experimental study to understand the behavior of Al 5083-H116 behavior with ogival nose shaped rods and 7.62 mm APM2 Projectiles. Residual velocity data and ballistic limit velocities were also computed.

Wang et al.[40] studied the dynamic response of impact on aluminum target protected or layered with alumina tiles. They observed that the conical shaped nose of the projectile that hits the target gets damaged and also the fracture pattern of cone shape develops in the nose of the projectile. They discovered that the optimum base plate thickness is a function of the damage evolution and material's failure mechanism e.g. Petalling, partial penetration, plugging, and indentation etc. They noted that the resistance capability of ceramics against ballistic impacts improves with the increase in ceramic plate thickness. Many researchers have also conducted extensive study in order to properly assess the performance of composite armors, soft laminates, fabric, and fibre reinforced composites [40]–[50].

Several research studies have been carried out in the past on the design and development of structures that can bear high intensity impulsive loads[2–7]. The face sheets are usually Aluminum or fiber reinforced polymers whereas the core is usually, wood, metal foams, polymers and metal honey combs. Radian et al. [13] found that monolithic plates offers more resistance to impact penetration because of their augmented resistance to bending loads. We may conclude from these research studies that the impact penetration and perforation resistance of sandwich constructions, as compared to other designs, is dependent on certain impact situations. In previous studies, core material and density have also been proven to be key factors/paramters and the selection of the proper material can optimize the performance of the structure. Both experimental as well as accurate numerical techniques are required to understand the material response and to improve the optimization process. Jamil et al[32], [33] showed that the energy absorbing characteristics increases with the increased impact energy. TPU can with stand high impulsive loads and be able to recover from high-intensity loading conditions.

Impact at High velocity such as ballistic impact cases involves strain rate dependent material deformation, erosion, and shattering. Therefore, a numerical model is required that takes into account the above mentioned effects to simulate the impact response effectively. With the advent of modern technology and computer programs the new numerical methods used by the researchers shows more realistic picture of impact response. Detailed literature review on the numerical simulation of ballistic impact problems shows that the most of the researchers are making use of continuum hydrodynamic codes to analyze the ballistic impact response [16], [18], [19]. Abaqus/CAE, Ls-Dyna, and Ansys AUTODYN are some of the most widely and successfully used explicit analysis tools to simulate the ballistic impacts of number of threat levels of different type of armors. Borvik et al. [20] investigated the impact behavior of cylindrical projectiles at high speeds on Weldox 460 E steel plate. Weldox 460 E steel was tested using Johnson Cook's plasticity and damage model. Because the projectile's material data was unavailable, the projectile was modelled using a linear elastic material model with an elastic modulus of 200 GPa and a poisson's ratio of 0.33. Buchar et al. [25] in the research analyzed the steel armor performance against ballistic impact of 7.62 mm AP projectile. Key factor behind success of the numerical results and experimental results closeness of this study is the use spall failure model for hardened steel projectile. Borvik et al. [21] determined the effect of projectile shape on ballistic performance in Ls-Dyna. Teng et al. [22] and Dey et al. [23] determined ballistic

performance of dual layered steels and the resistance of monolithic steel and Weldox 700 steel targets respectively. Johnson-Cook's plasticity and damage model were used for armor plate. One of the most comprehensive research on ballistic simulation was done by Borvik et al. [24]. He studied the performance of five different hardened steel alloys when struck by hard projectiles. On comparison with ballistic test results, very close correlation was found between experimental and simulation results.

2.5. INTRODUCTION TO FINITE ELEMENT CODES

Finite Element Analysis is the most credible and widely acceptable numerical procedure to examine the basic and complex mechanical problems. It has become a very powerful tool among the most essential and valuable apparatuses for researchers and designers in past years. The description of the problem and assignment of fundamental parameters are usually what determine the unwavering quality of numerical solutions. Many commercial Finite Element packages are now available that include simulation-based design approaches and make use of modern computational resources. Some of the well-known FE processors are ABAQUS, LS-DYNA, ANSYS, MATLAB, IMPETUS AFEA SOLVER, MSC DYTRAN, MSC NASTRAN, COMSOL, COSMOS, MSC MARC and many more. Pre-processors like MSC PATRAN, HYPERMESH and MENTAT are equipped with finite element models production facilities for the above mentioned FEA codes. In current research ABAQUS/CAE is utilized as a vital finite element analysis code to analyze the response of composite sandwich structures. ABAQUS CAE is widely acceptable and acclaimed software for Finite Element Analysis tasks.

2.6. Introduction to Abaqus Software

Abaqus was originally released in 1978 by Hibbitt, Karrisson and Sorensoen, Inc. Abaqus is a programme that visualizes the results of finite element analysis and is used to model and analyze complex mechanical systems. Abaqus is a suit for building finite element based models for solving different engineering related problems, which is not only capable for simple static or linear analysis but also can solve nonlinear or dynamic problems. Abaqus CAE has a graphical user interface for problem definition and solving. It can be used effectively to make or import geometries in a mesh-able regime. Abaqus CAE contains intense alternatives to work complex geometries and confirm the subsequent investigation model. Abaqus/CAE can be used to assign the material properties to the geometry, applying load, boundary conditions, and presenting the

finished model by making a job for analysis. The results of the analysis can be interpreted using the visualization module of Abaqus. There are two primary analysis modules of Abaqus/CAE.

- Abaqus Standard.
- Abaqus Explicit.

2.6.1. Abaqus/Standard

Abaqus/Standard, a universally useful examination module utilized as part of tackling an extensive variety of linear and nonlinear problems, including the static, dynamic, heat, and electrical behavior of materials. It is a general purpose solver that employs implicit integration schemes.

2.6.2. Abaqus/Explicit

Abaqus/Explicit is an extraordinary examination module of Abaqus /CAE, used for explicit dynamic analysis of finite element based models. Unlike implicit analysis, explicit analysis generates a time based solution after every small time interval rather than solving a system of mathematical equations after every increment. Abaqus/Explicit is extremely proficient for analyzing dynamic and transient loading cases, for example, blast and impact problems, and for simulation of nonlinear problems involving contact conditions.

2.7. Principles of Formulation

In this section, principles of formulation for numerical techniques are discussed. It involves,

2.7.1. Lagrange Formulation

One of the most sought after FEA formulation is lagrangian formulation technique commonly used in experimental operations. The basic characterization propagated by Lagrange formulation is that each body has unique nodal points. Elements are formed when nodal points are joined. When a change in shape occurs (i.e. a disfigurement of any sorts) the nodal points moves causing a change in shape.

One of the primary problem with conventional Lagrange-based formulations for impact perforation issues is excessive elements distortion. Mesh convergence study is necessary to accomplish a certain degree of unwavering quality. The material removal option can be used to

remove the extensively distorted elements, allowing the computation to proceed. The fact that small relocations and material contacts are shown with remarkable clarity is of enormous interest.

2.7.2. Euler Formulation

The Euler formulation is a widely used formula for studying moving materials or fluids, or for experiencing severe distortions. The Eulerian formulation is ideal for this purpose since the projectile and reinforcing material are subjected to such significant deformation and can approach the softening stage. The Eulerian formulation is supported by the spatial node points joining to create the elements. The mesh's elements move from one position to the next, creating mass, force, and vitality, and the material is referred to as a 'stagnant reference frame.' The Eulerian mesh must be big enough to capture all of the intricacies of material flow during deformation in order to use it.

2.7.3. Smooth Particle Hydrodynamics (SPH)

Smooth Particle Hydrodynamics technique is a computational method to simulate the mechanics of continuum media. It is a lattice free system that are connected for irregular issues having substantial and excessive distortions. From [51] , we may say that SPH overcomes the limitations of the Euler and Lagrange methods. The approach for function interpolation has cognizance of free nodal points with a changed mass, referred to as elements, for SPH formulation. In terms of introduction totals, a piece gauge allows you to portray the protection of mass, force, and vitality.

2.7.4. Dynamic Failure Models

The damage and material failure can be analyzed and demonstrated by the dynamic failure models in Abaqus. These failure models can be used for modeling of static and dynamic loading problems. In Abaqus/Explicit, there are two types of dynamic damage models that are appropriate for dynamic situations with a high strain rate. The key failure initiation criteria in the shear failure model is the material's plastic yielding. The ductile failure model uses elastic stacking of the material as the main failure initiation criteria. Failure models such as mentioned above can be utilized to restrain resulting load conveying limit of an element (up to the point of element removal) until the maximum value of stress is achieved. Both of the aforementioned models can be utilised for the same material at the same time.

2.7.5. Shear failure criterion

Shear based material failure criteria depends on the estimation of the proportional plastic deformation at element nodes i-e; damaged elements erode when the value of critical damage variable reaches 1. The damage variable is denoted by, **ω**, and is given by

$$\omega = \frac{\varepsilon_0^{pl} + \boldsymbol{\Sigma}\Delta\bar{\varepsilon}^{pl}}{\bar{\varepsilon}_f^{pl}} \tag{4}$$

Where, ε_0^{pl} defines initial value of plastic equivalent strain, $\Delta\bar{\varepsilon}^{pl}$ represents the plastic equivalent strain increment, $\bar{\varepsilon}_f^{pl}$ is the failure strain, and the overall damage parameter can be determined by summation of overall increments in analysis.

The failure strain, $\bar{\varepsilon}_f^{pl}$ depends on the plastic strain rate ($\dot{\bar{\varepsilon}}_f^{pl}$), stress ratio (p/q) (p is the stress due to pressure and q is the stress known as Mises stress), field variables and temperature. The shear failure model utilizes the proportionate plastic strain for failure initiation. It is intended for large strain rate misshaping of numerous materials. It can also be used with Mises as well as Johnson-Cook's plasticity models. Shera based material model can be utilized as a part of tensile based failure model.

2.7.6. Tensile failure criterion

The tensile failure criterion of Abaqus/Explicit uses the hydrostatic cutoff pressure to model dynamic spall for element failure. The tensile failure occurs when the cutoff pressure, p, increases from the hydrostatic cutoff stress of the material. The hydrostatic cutoff stress depends on temperature of element and the field variables. Hydrostatic cutoff stress does not have any default value.

With Mises and Johnson-Cook plasticity models, as well as equation of state models, the ductile damage model is employed. The tensile failure criteria is used to assess the damage caused by high strain rates in a variety of materials. To simulate element spall or a weight cutoff, this material model employs the hydrostatic weight as a disappointment scale. It may be used as part of Mises, Johnson Cook Plastic, or equation of state models, just like shear failure models. It may be incorporated into a shear failure model.

2.8. Failure decisions

When the elastic or tensile failure initiates at the nodal point, the material elements fails. There are five choices available in the tensile based failure criteria which offers element failure at nodal points, these choices include,

- Element removal (Default choice), which erodes the elements on failure
- Four spall models, which depicts the material failure by shock wave generated from the rare face of the impacted material.

2.8.1. Element removal

At an integration point when the tensile failure occurs, all the stress components are assigned a value of zero and the material failure occurs at this point. The element of the material will be removed, whenever the tensile failure variable reaches a value of 1. For complete failure of material all the elements are not necessary to fail or erode. In first-order solid elements, the elements erosion takes place whenever nodal point fails. In shell elements, all the nodal points along the thickness must fail in order to cause the element removal from the mesh. For second order beam elements, when all of the nodal points fail at one of the two element integrations along the beam's axis, the beam fails. Similarly, the triangular and tetrahedral elements fail when anyone of nodal point fails.

2.8.2. Spall models

Spall (the material disintegration) model is an alternative failure choice in which, instead of element removal, there are four alternate choices available. This category involves four failure combinations. At an integration point when the tensile failure occurs, it may or may not set the deviatoric stress components to zero, similarly the cutoff pressure may or may not be limited by the hydrostatic cutoff stress. Therefore, four failure combinations are possible which are as follow,

Ductile shear and ductile pressure: The stress components are unchanged, and the hydrostatic cutoff stress determines the pressure stress.

Brittle shear and ductile pressure: the components of stress become zero and will be zero for the remaining analysis, and the pressure stress is given by the hydrostatic cutoff stress.

Brittle shear and brittle pressure: the components of stress become zero and will be zero for the

remaining analysis, and the pressure stress is given by compressive stress.

Ductile shear and brittle pressure: the stress components remain unchanged, and compressive stress determines the pressure stress.

3. Chapter 03: Materials and Modeling

3.1. Material Properties and Dimensions

Abaqus/CAE, a finite element technique software, was utilized for numerical simulations. Lagrange method of spatial discretization was used for numerical analysis because according to the study conducted by [30]. When compared to mesh-free approaches like Smooth Particles Hydrodynamics, the Lagrange method produces substantially better results. Only issue that appears is that the mesh becomes excessively distorted in Lagrange method, which results in simulation errors which leads to termination of simulation or have a substantial impact on the accuracy of the results. Thus mesh size is an integral part of numerical analysis.

Two materials were chosen for the impact analysis in this study which are,

- Aluminum Alloy Al-5083 H-116
- Thermo-plastic Polyurethane TPU

1. **Aluminum Al-5083 H-116** is an aluminum-magnesium alloy majorly used for naval structures and for ballistic protection purposes. Aluminum alloy Al-5083 H-116 was chosen due to its high strength properties. Aluminum Al-5083-H116 is used as a face sheet material in this study. Some mechanical characteristics for aluminum alloy armor plates are specified by the US Army Research Laboratory [30]. The following mechanical characteristics are recommended for AA5083-H116 plates: ultimate tensile strength σ_u = 283 MPa, yield strength determined by the 0.2 percent offset σ_0=200 MPa, and percent elongation at tensile failure ε_f =0.10. Mechanical properties of Al-5083- H116 are tabulated in **Table 1**.

2. **Thermo-plastic polyurethane TPU** belongs to polymers family and it is used as a core material in sandwich structures in this study. Polymers are widely used for many purposes due to its cheapness, corrosion resistance, production ease and relatively low density. Highly ductile behavior and stress - strain recovery under tensile tests, TPU is one of the most useful and flexible plastic material in its family. Under impact loading, TPU energy absorption increases proportionally with increased impact loading. TPU can also recover from extreme loading conditions, whereas metal-based cellular solids like honeycomb cores are unlikely to do so. Mechanical properties of TPU material are tabulated in **Table 3**.

3.2. Dimensions

Dimensions of Aluminum Al-5083 H-116 are taken from the standards mentioned in NATO Stanag 4569 standard [30]. Similarly the Core material TPU dimensions are taken same as that of Aluminum Al 5083- H116. Both the face sheets and core material are according to NATO standards for ballistic impact testing. The sandwich structure is 400 x 400vmm^2 in dimensions. There is no adhesive or chemical material between the face sheets and the core material because it is mechanically bonded to them. Projectile dimensions are taken from [54].

The material properties and the Johnson-Cook's plasticity model parameters of aluminum face sheets are given in **Table 1** . Mie-Gruneisen EOS parameters for aluminum sheets used in this simulation are tabulated in **Table 2**. Johnson cook's failure model parameters for base armor plate are also given in **Table 2**. The material properties Ductile damage and failure criterion parameters are tabulated in table 3. Isotropic hardening data for TPU is tabulated in **Table 4**.

Table 1

Mechanical Properties of Al 5083 - H116 Face sheets

Parameters	**Symbol**	**Unit**	**Al 5083 - H116**
Density	ρ	Kg/m^3	2700
Elastic modulus	E	GPa	-
Shear modulus	G	GPa	70
Poisson's ratio	ν	-	0.3
Initial yield stress	A	MPa	167
Strain hardening coefficient	B	MPa	596
Strain rate coefficient	C		0.001
Strain hardening exponent	n		0.551
Reference strain rate	$\dot{\varepsilon_o}$	1/s	1

Thermal softening exponent	m		0.859
Specific heat at constant pressure	C_p	J/kg.K	910
Room temperature	T_r	K	293
Melting temperature	T_m	K	893
J-C Failure	D_1	-	0.1
	D_2	-	0.4
	D_3	-	-1.3
	D_4	-	0.05
	D_5	-	0
	$\dot{\varepsilon_o}$	1/s	$1x10^4$

Table 2

Mie Gruneisen EOS parameters for Al 5083 - H116 Face sheets

Parameters	**Symbols**	**Units**	**Al 5083 H116**
Density	ρ	Kg/m^3	2700
Elastic wave velocity	C	m/s	5340
Slope values	S	-	1.40
Gruneisen Coefficient	γ	-	1.97

Table 3

Mechanical Properties of Thermoplastic Polyurethane TPU Core

Parameters	**Symbols**	**Units**	**Thermoplastic Polyurethane TPU**
Youngs' modulus	E	MPa	158

Poisson's ratio	ν		0.40
Density	ρ	Kg/m^3	1150
Strain rate	$\dot{\varepsilon_o}$	1/s	0.001
Fracture strain for ductile damage		-	2.9
Stress traxiality		-	0.33

Table 4

Isotopic Hardening data for Thermoplastic Polyurethane

Yield stress (MPa)	11.05	25.92	45.36	119.02	265.26	295.43	390.17
Plastic strain	0	0.36	0.76	1.42	1.90	2.18	2.97

3.3. Finite Element Analysis

In finite element analysis, materials behavior is analyzed by characterizing the material into small discrete elements. Spatial discretization requires a variety of numerical methods. Commonly used techniques for discretization of material are Euler, Lagrange, ALE (Arbitrary Lagrange Euler, a mixture of Euler and Lagrange), and meshless techniques like SPH (Smooth Particles Hydrodynamics). In comparison to the meshless SPH approach, the Lagrange methodology appears to be the most appropriate tool for analyzing deformations. The material mesh moves with the movement of the material in the Lagrange method, which is perfect for capturing material movement and features in areas with little deformation. Because of its ability to trace material interactions precisely and effectively, this detailing is widely used. The drawback of Lagrange technique is that the numerical mesh can become highly deformed or knotted in an

incredibly disfigured area, causing unwanted effects on the time step and accuracy. Excessive element distortion leads to zero and negative volume error for some cases. These issues may be solved by using a different and more effective meshing approach, which may require more computing power but improves the output results substantially.

Numerical models used in this numerical analysis are,

3.4. Ductile Damage

The Ductile Damage Initiation Criterion is a model for predicting ductile metal damage initiated by nucleation, growth, and void's coalescence. The model assumes that the equivalent plastic strain at the start of damage is a function of stress triaxiality and strain rate. The ductile criterion can be used in conjunction with the Mises, Johnson-Cook, Hill, and Drucker-Prager plasticity models, as well as the equation of state. Parameters of ductile damage criterion for Thermoplastic Polyurethane TPU are tabulated in **Table *3***.

3.5. Damage Evolution

3.5.1. Displacement

Displacement damage evolution to define the damage as a function of displacement after damage initiation. It defines damage in terms of displacement in cohesive elements for elastic materials.

3.5.2. Energy

Energy damage evolution defines damage in terms of the energy required for failure (fracture energy) after the initiation of damage.

3.6. Johnson Cook plasticity model

Johnson Cook's plasticity model is a well-known model used for high strain rate dependent problems [52] . Johnson-Cook's model is available in commercial FE analysis software packages and is most used for the ballistic impact numerical simulation studies. This model particularly describes the rate dependent in elastic behavior of ductile materials. J-C model also describes the effects of strain, strain rate hardening and thermal softening on the flow or yield stress of the material. Johnson Cook's ductility model is expressed as,

$$\sigma = [A + B\varepsilon^{n}][1 + C\ln\dot{\varepsilon}^{*}][1 - (T^{*})^{m}] \quad (5)$$

The term "εp" represents the equivalent plastic strain rate, "ε^*" is the ratio of equivalent plastic strain rate to reference strain rate i.e. "$\varepsilon^* = \dot{\varepsilon}_p / \dot{\varepsilon}\ °$", and T^* is the Normalized Temperature term and is expressed as,

$$T^* = \frac{(T - T_{ref})}{(T_{melt} - T_{ref})} \tag{6}$$

where T_r is the room temperature and T_m is the melting temperature. A, B, C, n and m in J-C plasticity model are the experimentally determined material constants where A is the initial yield stress, B is the coefficient of strain hardening, C is the coefficient of strain rate, n is the strain hardening exponent, and m is thermal softening exponent.

3.7. Johnson Cook Damage Model

The Johnson Cook Damage model is a fracture strain model that includes the effects of temperature, stress triaxiality, and strain rate on material fracture strain. The material fails when the damage variable reaches a critical value, according to the JC failure model. This damage variable is defined as,

$$D = \sum \frac{\varepsilon p}{\varepsilon f} \tag{7}$$

The damage parameter "D" can be 0 or 1. If the the material is undamaged then D = 0 and if the material is fractured then D = 1. According to J-C failure model, the strain energy is expressed as,

$$\varepsilon^{pl} = \left[d_1 + d_2 e^{(-d_3 \eta)} \right] \left[1 + d_4 \ln \left(\frac{\dot{\varepsilon}^{pl}}{\dot{\varepsilon}_0} \right) \right] (1 + d_5 T^*) \tag{8}$$

Here d_1, d_2, d_3, d_4, and d_5 represents the temperature strain rate and strain rate hardening dependent material constants

3.8. Mie-Grüneisen equation of state

The Mie–Grüneisen equation of state is an equation that describes relationship between a solid's pressure and volume at a given temperature. It's used to find out the pressure in a shock compressed solid. In this numerical simulation, the Mie-Grüneisen equation of state is employed. This Mie-Grüneisen EOS represents materials that are subjected to high pressures. Parameters of Mie-Grüneisen EOS for Aluminum plate are tabulated in **Table *2***.

3.9. Plasticity modeling for Thermoplastic Polyurethane

Thermoplastic Polyurethane TPU can be modelled using Cowper – Symonds power law by considering it as an isotropic elastic – plastic material that exhibits strain rate dependency. Total strain-rate can be disintegrated into an elastic component, *el*, and a plastic component, *pl*. and the plastic flow stress as σ_{pl}, of a material which can be expressed as,

$$\sigma_{pl} = f(\varepsilon_{pl}).R(\dot{\varepsilon}) \tag{9}$$

Where f represents quasi-static stress - strain behavior of material which is acquired from stress strain curve. Stress strain behavior can be introduced into Abaqus from stress strain curve values. R is the ratio of the yield stress at any strain-rate to the static yield stress and $E^{\cdot}$ denotes the strain.

Cowper-Symonds model which is used to incorporate the strain rate effects in TPU as follows,

$$\dot{\varepsilon}_{pl} = D(R-1)^{p} \tag{10}$$

The power-law relationship is given as follow,

$$\sigma_s = \sigma_0 \left[1 + \left(\frac{\dot{\varepsilon}_{pl}}{D}\right)\right]^{\frac{1}{p}} \tag{11}$$

Here, $\dot{\varepsilon_{pl}}$ represents the strain-rate and, σ_s and σ_0 denotes the yield stress at the higher strain-rate and the static yield stress, respectively. *D* and *p* are the material parameters, which can be determined by Regression procedure from Split Hopkinson Pressure Bar tests data. D and p are the coefficients for the Cowper Symonds power law. The values of these two coefficients (D & p) are 971 s^{-1} and 0.98, respectively. These values were determined from SHPB data from tests. The

material properties and isotropic hardening data for TPU are listed in **Table 3** and **Table 4**, respectively. Ductile failure criterion available in ABAQUS/Explicit [50] is used to simulate failure of the TPU.

Prior to the impact simulations, the TPU's mechanical response was simulated under in-plane tensile load. **Figure 7** shows the load-displacement graph, for the TPU under in-plane tensile loading conditions simulated in Abaqus.

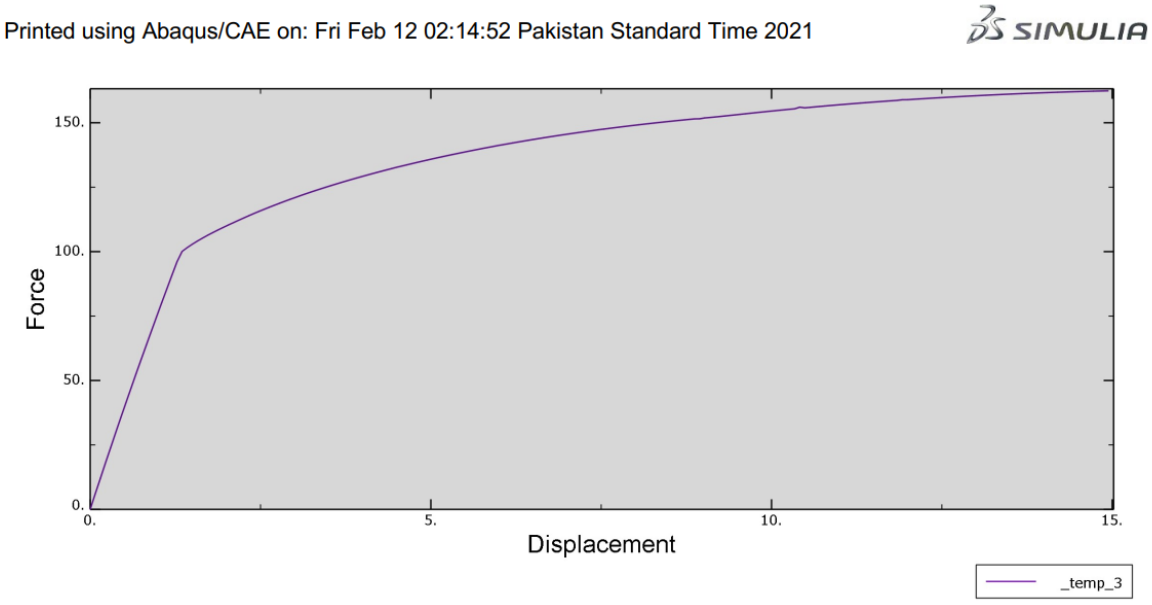

Figure 7: Load vs Displacement graph of TPU under tensile load

3.10. Sandwich Structure

Sandwich structures used in this research study are comprised of Core material and front - back face-sheets. The Polymer based core material is sandwiched between the two aluminum face sheets. The areal dimensions in all the cases are same while the thickness of the structure varies. A visual representation of sandwich structure is given in **Figure 8**.

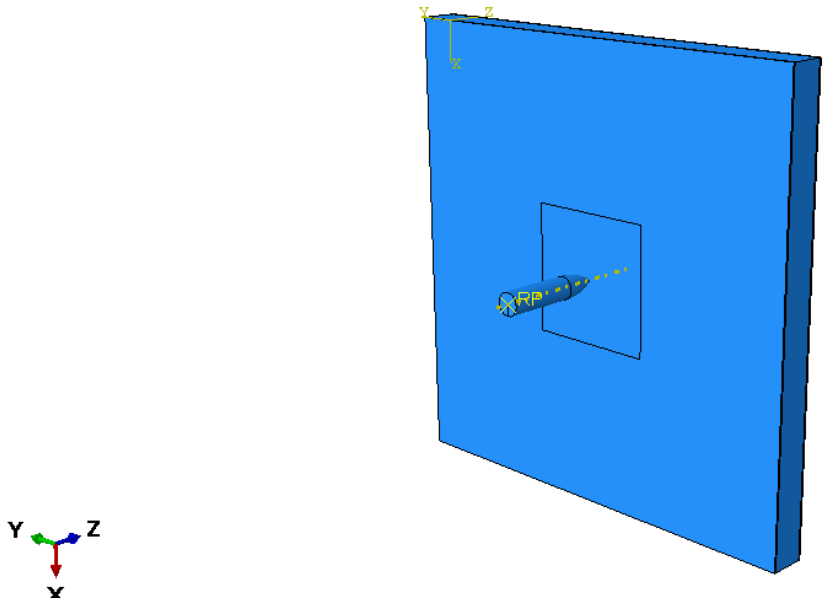

Figure 8: Sandwich Structure

3.10.1. Aluminum Al-5083-H16 Face sheets

Face sheets used in this research study are Aluminum Alloy Al-5083 H116. The areal dimensions of the sheets are 400 x 400 mm^2 which is accordance with NATO stanag 4569 standard [55]. The thickness of the face sheets varies are 1.2 mm, 1.5 mm and 2 mm. Each of them are used in different case studies in this research.

3.10.2. Thermo-plastic Polyurethane Core

Core material used is this material is Thermo-plastic polyurethane polymer. The areal dimensions are same as that of face sheet that is 400 x400 mm^2. The thickness of the cores are 20 mm, 30 mm and 50mm. Each of them is used in different case study of this research.

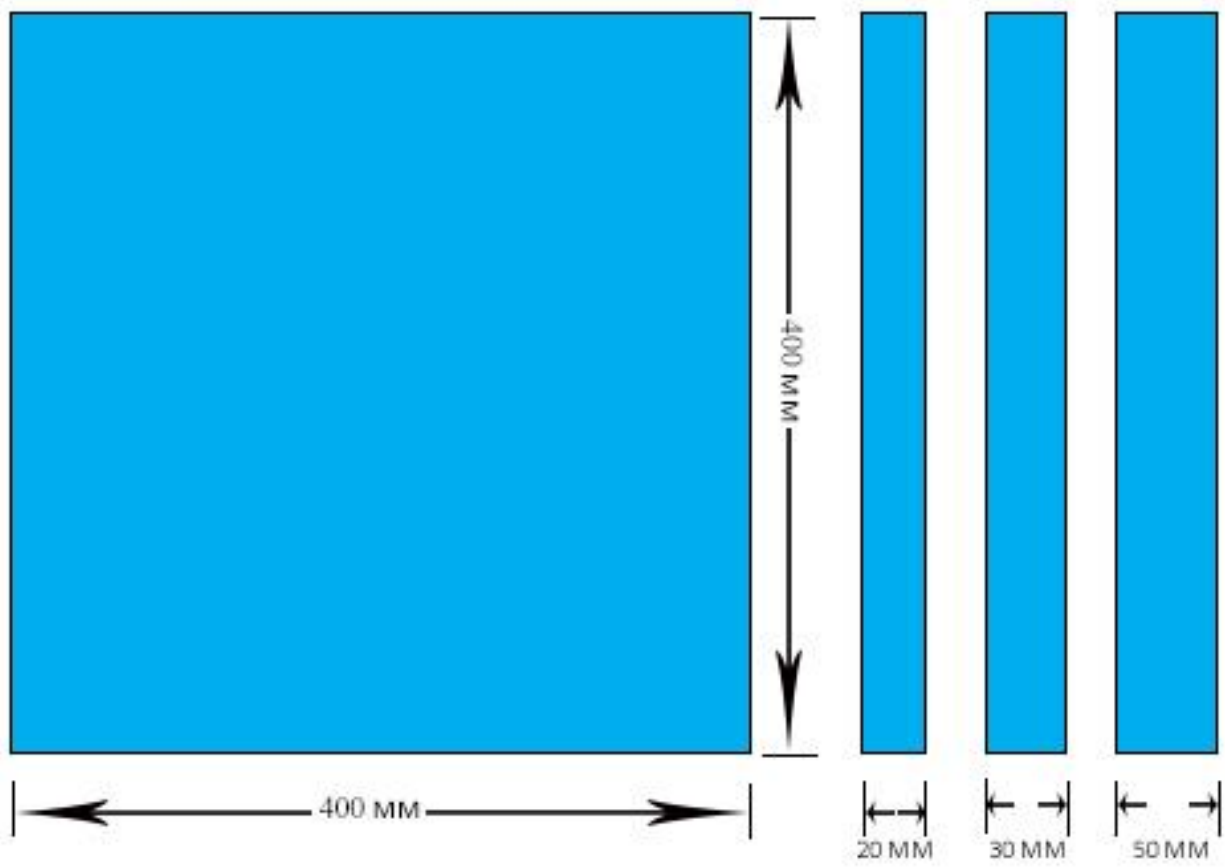

Figure 9: TPU Core with different thicknesses

3.11. Projectile

Projectile used in this study was modelled as analytical having mass of 52.5 grams and 19mm Diameter. The projectile dimensions is taken from [54]. In numerical simulations, initial projectile velocity ranges from 66.3 - 360.30 m/s.

3.12. Mesh

The meshing methodology acquired in the analysis of current impact problem involves a continuous mesh that transitions from coarser mesh to fine mesh depending upon the region of interest. This method involves the partitioning of face sheets and core material regions. Each part

is seeded with appropriate mesh density in the individual region based on the required refinement and continuum behavior in the results. The projectile is also meshed finely for the accurate results.

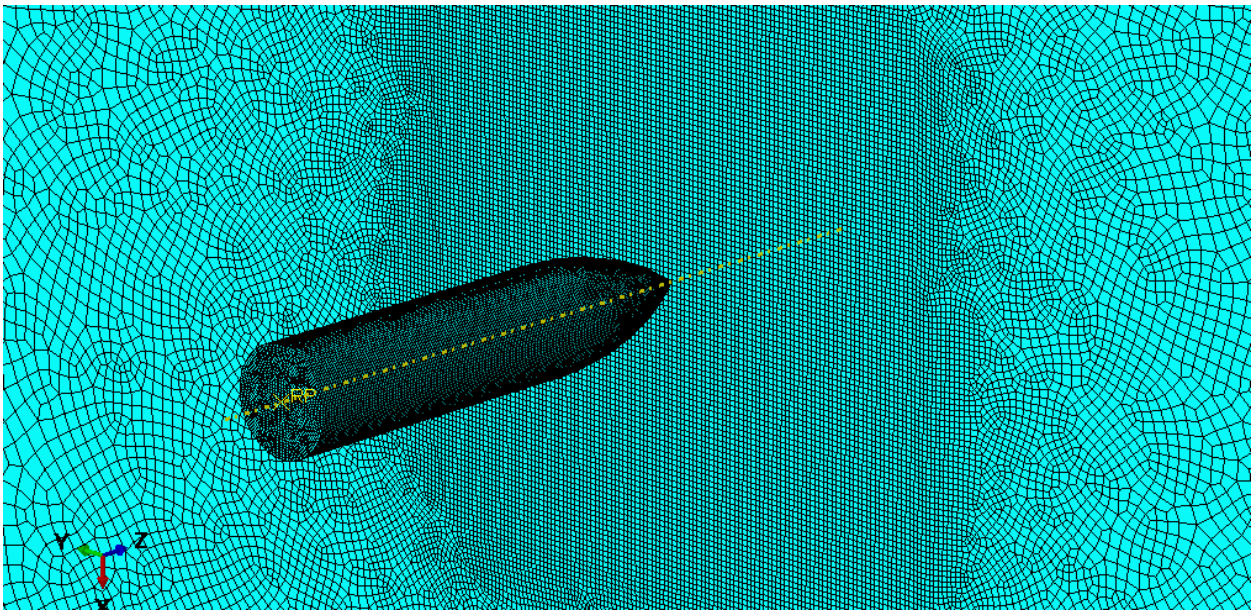

Figure 10: Mesh on sandwich structure

3.12.1. Aluminum Face sheets

The meshing module uses an 8-node linear brick with reduced integration (C3D8R) and hourglass control elements to mesh aluminium face sheets. Face sheets are partitioned in two regions, the mesh size was adjusted in these regions based on the area of interest. Elements size for the face sheets ranges between 1 mm to 5 mm, whereas the element size of 1 mm was used along the thickness of the plate. In each cross sectional direction, the element size is assumed to be small in the impact zone and gradually grows away from the impact region. The elements size for face sheets is very critical in the current model because much smaller or larger elements can cause different stiffness issues in the model of face sheet.

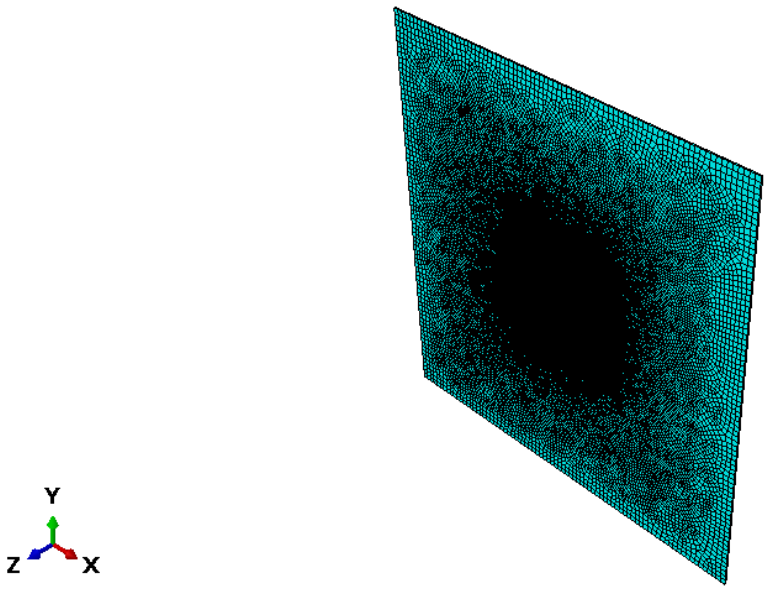

Figure 11: Mesh on Al-5083-H116 face sheet

3.12.2. Thermo-plastic Polyurethane core

TPU Core was meshed with 8-node linear brick, reduced integration with hourglass control elements of different sizes in two regions of plate. These regions were defined by partitioning the plates into two parts. Elements size for the core material ranges between 1 mm to 5 mm whereas the element size of 5 mm was used along the thickness of the plate. The elements size for core material is very critical in the current model because much smaller or larger elements can cause different stiffness issues in the model of core material. Element mesh size increases from impact region to away from center along the cross sectional direction

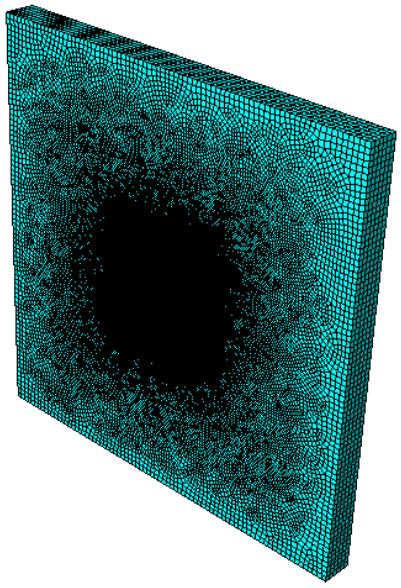

Figure 12: Mesh on TPU Core

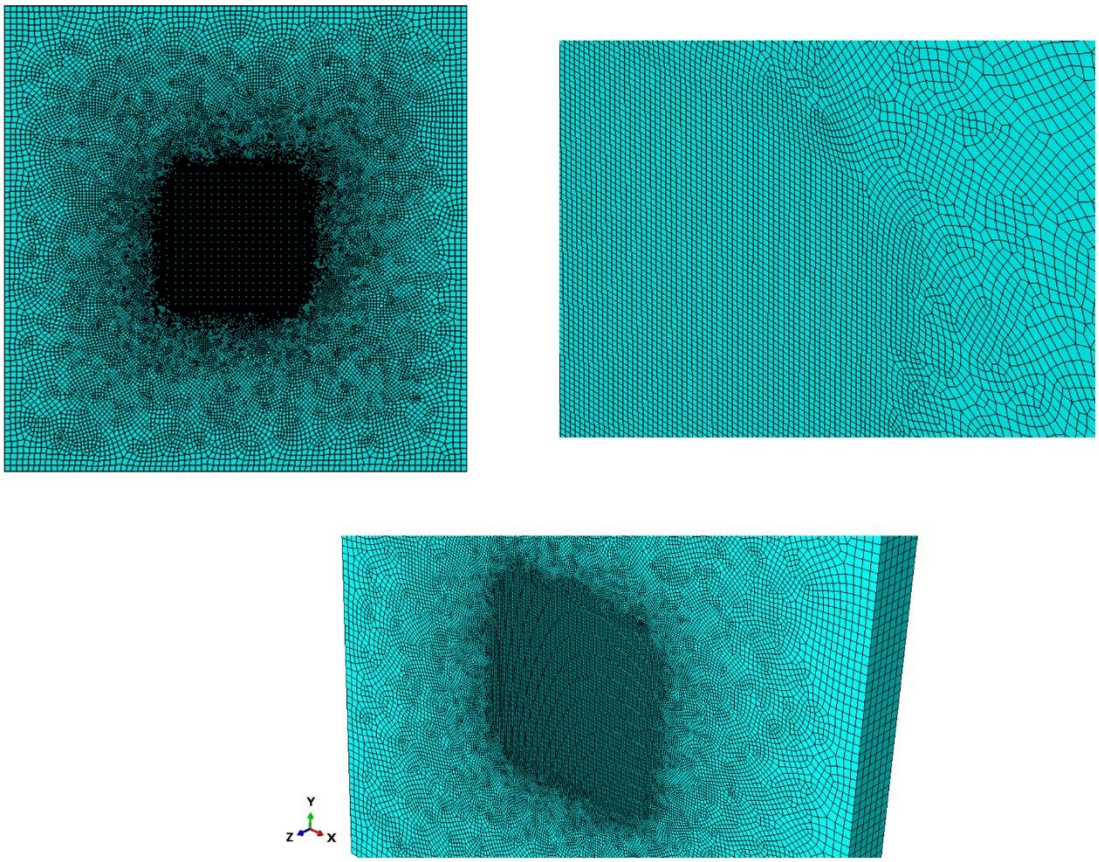

Figure 13: Different orientations of mesh on TPU core

3.12.3. Projectile mesh

Projectile was meshed with using 8-node linear brick, reduced integration (C3D8R) with hourglass control elements (structured mesh) by the meshing module in three regions. The mesh size was adjusted in the area of interest. Elements size for the projectile ranges between 0.5 mm to 1 mm along the length of the projectile.

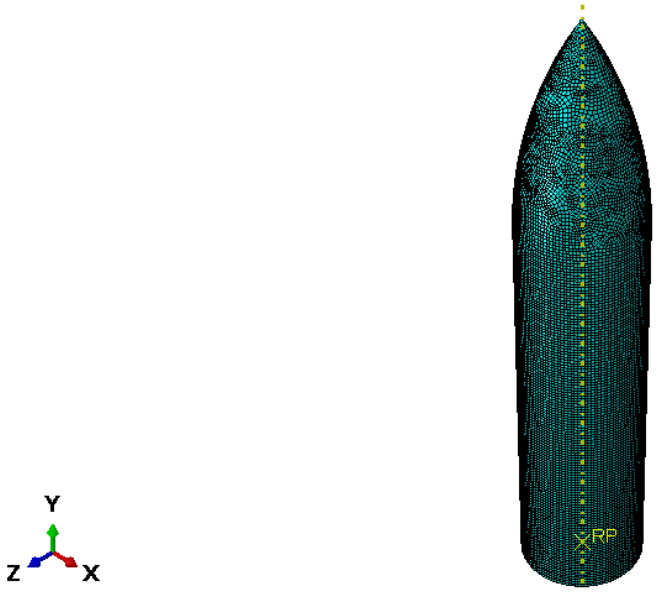

Figure 14: Mesh on Projectile

3.13. Boundary and Contact Conditions

Sandwich structure is fully clamped/fixed at its exterior edges and all its degrees of freedoms are zero. The Abaqus kinematic contact method was used to assign contact between the projectile and the target structure. Between the face sheets and the core material, general contact (explicit) was used. Between the projectile and the sandwich structure, surface to surface (explicit) contact was assigned (face sheets and Core). In contact definition, the projectile surface was treated as a master surface, while the face sheets and core were treated as a nodal-based slave surface.

3.14. Setting up the model

Sandwich structure compromising of face sheets and core material was constrained at its edges. The projectile was normal to the plate with its tip touching the face sheet. The contact definition was hard contact for normal objects. The initial velocity of the projectile varied with each new case. Similarly the configuration of sandwich structures also varied with different cases.

For the face sheets and the core, a three-dimensional finite element model was created. Eight node continuum hexahedral elements with reduced integration formulation were used as the mesh type (C3D8R).The projectile impact is an extremely localized phenomenon. To save the computation time, the mesh size was refined and smaller near the center, while the mesh size for the areas

increased as the distance from the centre of the plate increased using biased meshing. Elements size for the face sheets and core ranges between 1 mm to 5 mm, whereas the element size of 1 mm was used along the thickness of the face sheets. In order to prevent the Projectile from unrealistic distortion, distortion control alongside enhanced hour glassing properties were used in the simulation.

4. Chapter 04: Results and Discussions

To model the numerical setup as an accurate finite element model, it was necessary to create a model that is based on prior experiments. The work done by Borvik [15] on the perforation of AA5083-H116 Aluminum armor plates with ogive-nose shape rods, 7.62 mm APM2 bullets was considered as a reference. The material model parameters and Johnson cook's material model parameters were taken from [56] , [57] for Aluminum 5083-H116.

Table 1 contains the Johnson cook's material parameters for Aluminum 5083-H116. Mie – Gruneisen EOS parameters were taken from [58] and its parameters are listed in **Table 2**. Prior to the impact simulations, the TPU's mechanical behavior was simulated under in-plane tensile stress. The computed load-displacement graph for the TPU under in-plane tensile stress conditions is shown in **Figure 7**. **Figure 7** shows that the simulated mechanical response validates the data available in literature [33].

4.1. Validation models

To accurately model the simulation, setting up the simulation as done by the [59] was considered to validate his results for Weldox 460E and residual velocities were validated with the already available data in [59] , [21]. This task was done to model the simulation accurately and in perfect manner. Validation results for Weldox 460E are listed in **Table 5**. After making an accurate simulation, material model for Aluminum 5083 – H116 was also validated in accordance with work done by Borvik [15] against 7.62 mm APM2 bullets; a 20mm Aluminum 5083-H116 plate impacted by a 7.62 mm AP core at 741m/s. The results are compiled in **Table 6**.

Table 5 : Numerical Model Validation for Weldox 460E

Initial Velocity In Literature [21]	**Axis-Symmetric Numerical Results with Adaptive Meshing [21]**	**3D Numerical Results without Adaptive Meshing** [59]	**3D Numerical Results of Present Validation Model**
600	523.00	555.04	541.31
405.70	304.00	332.64	338.05

Table 6 : 20 mm Aluminium-5083 – H116 against 7.62mm AP Projectile

Initial Velocity (m/s) in Literature [15]	Residual Velocity (m/s) in Literature [15]	Residual Velocity (m/s) in Present Validation Model
741	532	537.12

4.2. Ballistic Impact

In present study, composite sandwich structures of variable thicknesses were developed to test against 12.7 mm Ogival nose shaped projectiles. Numerical simulations on Abaqus Software were developed to find out the ballistic limit velocities of sandwich structures. This study was conducted to find out the impact perforation and penetration resistance, ballistic limit velocities, effect of core and face sheets thickness on structural integrity and performance and failure mechanisms in sandwich structures during impact loading in different configurations of sandwich structures.

In sandwich structures, thickness of the face sheets are 1.2 mm, 1.5 mm and 2 mm while the core material thickness was 20 mm, 30 mm and 50 mm. There were total of 9 different sandwich structures and their configurations are listed in **Table 7**.

Table 7 : Different Configurations of Sandwich Structures

Sandwich Structures	TPU Core 20 mm	TPU Core 30 mm	TPU Core 50 mm
Aluminum FS 1.2 mm	1.2 x 20 x 1.2 mm	1.2 x 30 x 1.2 mm	1.2 x 50 x 1.2 mm
Aluminum FS 1.5 mm	1.5 x 20 x 1.5 mm	1.5 x 30 x 1.5 mm	1.5 x 50 x 1.5 mm
Aluminum FS 2.0 mm	2.0 x 20 x 2.0 mm	2.0 x 30 x 2.0 mm	2.0 x 50 x 2.0 mm

These configurations are divided in 3 cases which are further subdivided in 3 types for the ease of discussion which are as follow,

Case 1 includes 1.2 mm thick face-sheet panels with all three core thicknesses. 1.2 x 20 x 1.2 mm, 1.2 x 30 x 1.2 mm , 1.2 x 50 x 1.2 mm sandwich panels configurations are included in this

case. Each configuration is named as a type 1, type 2 and type 3 respectively to further discuss the results with ease.

Case 2 includes 1.5 mm thick face-sheet panels with all three core thicknesses. 1.5 x 20 x 1.5 mm, 1.5 x 30 x 1.5 mm , 1.5 x 50 x 1.5 mm sandwich panels configurations are included in case 2. Each configuration is named as a type 1, type 2 and type 3 respectively to further discuss the results with ease.

Case 3 includes 2 mm thick face-sheet panels with all three core thicknesses. 2 x 20 x 2 mm, 2 x 30 x 2 mm , 2 x 50 x 2 mm sandwich panels configurations are included in case 3. Each configuration is named as a type 1, type 2 and type 3 respectively to further discuss the results with ease.

4.2.1. Ballistic Impact Testing

In this section, ballistic response of sandwich structures against 12.7 mm ogival nose shaped projectile is discussed for each case. There were total nine different sandwich structure configurations and each sandwich structure was impact tested for different velocities ranging from 360.30 – 66.00 m/s. The ballistic limit velocity, which shows the lowest impact velocity necessary for a projectile to completely perforate a target, is mostly used to evaluate sandwich panel perforation resistance [60]. Ballistic limit velocities were found out in each case. The highest impact velocity, Vi, where the residual or rebound velocity, Vr, equals zero is designated as the ballistic limit velocity, VBL (i.e. no full penetration). The effect of the projectile's impact velocity, Vi, on its residual velocity, Vr, and velocity drop, Vd, is listed.

4.2.2. Factors affecting Ballistic Impact

Target configuration is an important parameter on the protective performance which is increased by increasing the thickness of target. Effect of core and face-sheets thicknesses are discussed separately as follow,

4.2.2.1. Effect of core thickness

Influence of Core thickness on the overall performance of sandwich structure is discussed in this section. Core material and its thickness plays a vital role on the impact penetration and perforation resistance against projectiles during high speed impact. The thickness and density of the core are both influential factors in the construction of sandwich panels. The core plays a

critical part in the panel's energy absorption capabilities when it is hit at a low speed. By keeping the face-sheets apart to generate an evenly stiffened sandwich panel, the core resists shear force and enhances structural stiffness. As thermoplastic polyurethane TPU is one of the most versatile polymer material in its family of polymers, it exhibits high ductility and can withstand high impulsive loads upon high velocity impact. The increase in core thickness provides additional strength to the structure along with increased damage resistance. Ballistic limit velocities were found to be decreasing as core thickness increased. Increase in the impact resistance of 30.6% and up to 40.8% with the increase in core thicknesses of 30 mm and 50 mm, respectively is observed. Ballistic limit velocity is found out to be highest in structures with thicker core. **Table 8**,**Table 9** Table **10** presents the numerical results of the residual velocity and velocity drop values for all three cases and their subsequent types.

4.2.2.2. Effect of face-sheet thickness

Influence of the face-sheet thickness on the overall performance of sandwich structure is discussed in this section. As the sandwich cores are of usually soft and less dense material to lower the weight of the overall structure. In contrast, face-sheets are usually made of strong material so they can bear more impulsive load and give enough strength by carrying all the bending stresses acting onto the structure. When the sandwich panel is subject to impacting load, the upper face-sheet confronting the projectile experiences the compressive load while the bottom face-sheet experiences the tensile load. The front face-sheet experiences the damage due to compressive loads pushing the core to the back resulting in debonding of face-sheet with the core. The face-sheet at the back side will stay intact with the core while experiencing tensile load at the back face. A thicker face-sheet will deform less as compared to the thin face-sheet as the deformation area associated with bending deflection increase on the face-sheets. A thinner face sheet can be penetrated more easily at high speed impact before its deformation extends to larger area. With increasing face-sheet thickness, impact resistance and ballistic limit velocity are found to increase. Increase in the impact resistance of 11.7% and up to 18.2% with the increase in face-sheet thicknesses of 1.5 mm and 2.0 mm, respectively is observed. The ballistic limit velocity is highest in the structure which has thicker face sheets and core.

4.3. Investigation of failure and damage resistance

In this section, structural response to impact penetration, damage resistance against projectile and failure phenomena is discussed in detail. According to US Army standards, perforation is achieved if the projectiles is embedded in target but light can pass through it. However, US Navy defines perforation when the projectiles fully emerges out from the target [61]. Based on these standards, **Figure 15** shows perforation according to US Army standard where as partial penetration according to US Navy standards. In this research study, we have considered US Navy standard for the evaluation of deformation after impact.

Three standard failures statuses were found based on numerical results, corresponding to projectile rebounded from, lodged in, and perforate the sandwich panel. The geometric characteristics of sandwich structures, as well as the impact velocity, have a key role in the penetration process and failure. Ballistic limit velocities were found out for each configuration type and structural behavior to failure and damage resistance is observed. **Figure 22** represents the Progression of the projectile through the composite sandwich structure at various time intervals. The projectile comes in contact with the front face skin and pushes it backwards bending the sandwich panel to the back. The front skin experiences the compressive force and projectile starts to penetrate in. As the projectile breaks in the front face skin, core starts debonding from front face sheet while the rear face sheet still stay bounded to the core. The projectile penetrates through the face skin and then penetrates trough the core as well. The rear face sheet deformed marginally due to the bending of sandwich structure. Face-sheets are completely debonded from core when the projectile completely perforates the structures and exist from rear side. This behavior is commonly observed in all the structures which were studied in this research work. **Figure 16** shows a half cut view of fully perforated sandwich structure when impacted at 293.4 m/s velocity.

The study reveals that the mechanics of perforation are extremely intricate and are dependent on a number of variables such as target thickness, target material characteristics, and projectile geometry. The impact velocity of the bullet has a significant influence on the target deformation. With increased impact velocity, the global deformation was observed to decrease. The target exhibits higher global deformation at low velocities. The highest global deformation was found to be highest at the ballistic limit velocities of the structures.

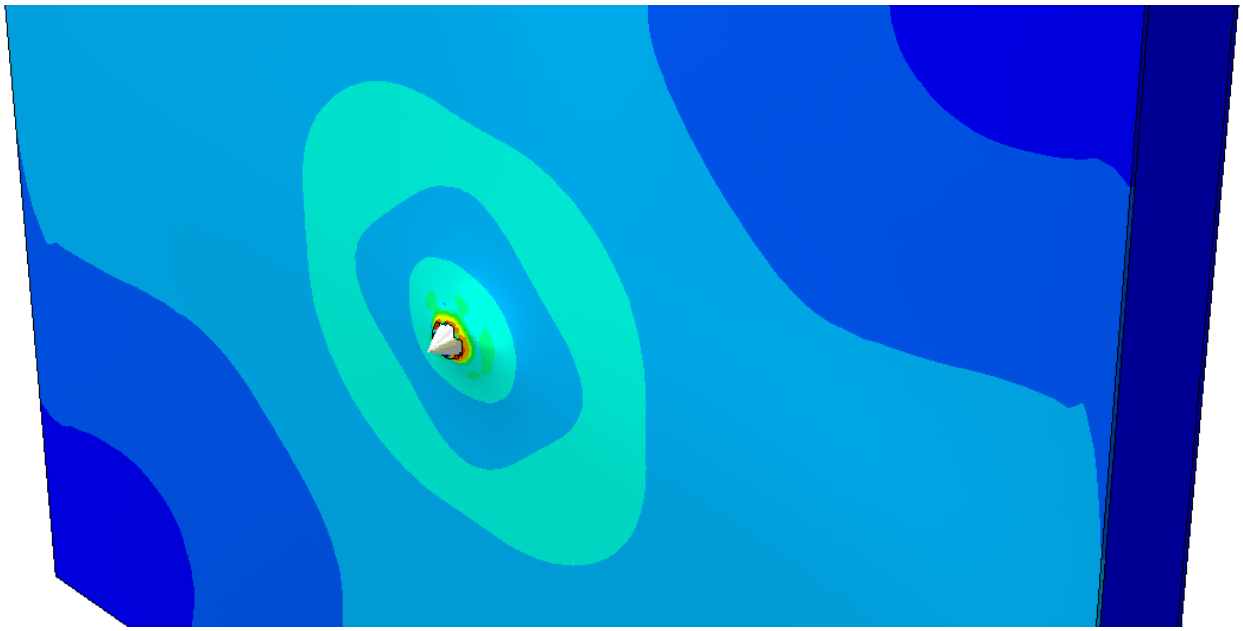

Figure 15 : Perforated Structure as per US Army Criterion

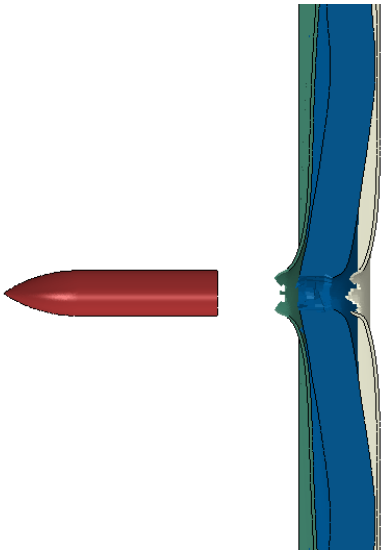

Figure 16 : Fully Perforated Sandwich Structure

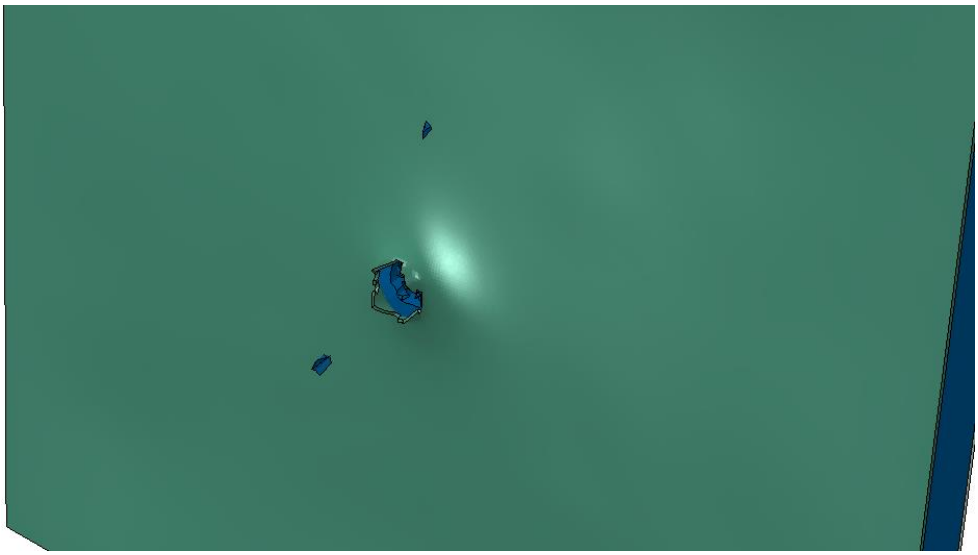

Figure 17 : Formation of Fragmentations in Core

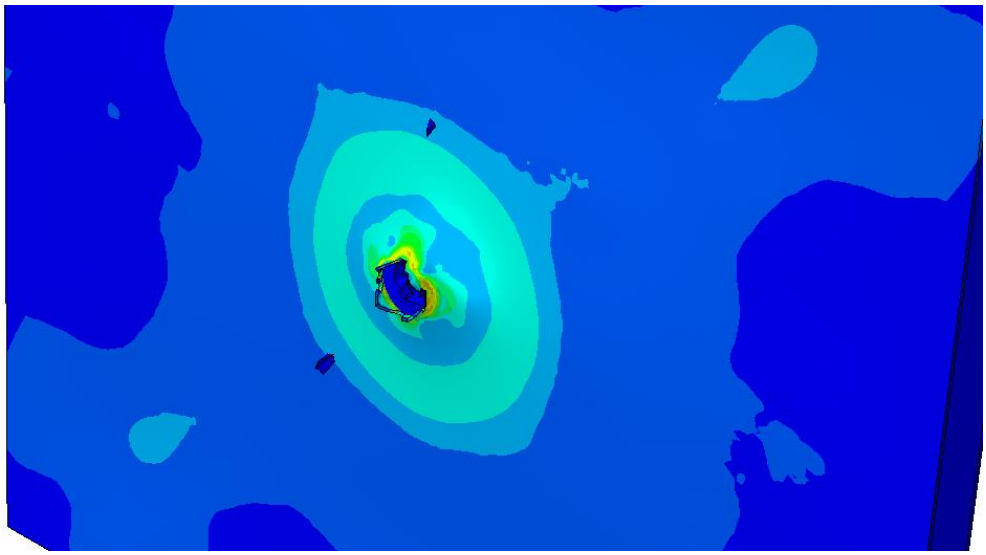

Figure 18 : Formation of Petals in Face sheets

Total nine different variations of sandwich panels were taken into consideration to study their behavior against 12.7 mm AP Projectile. These nine configurations are further classified into general cases based on their core and face-sheet thicknesses. Damage resistance and failure phenomena in each case is discussed as follow,

Case 1 includes 1.2 mm thick face-sheet panels with all three core thicknesses. 1.2 x 20 x 1.2 mm, 1.2 x 30 x 1.2 mm , 1.2 x 50 x 1.2 mm sandwich panels configurations are included in this case and they are entitled as type 1, type 2 and type 3 respectively. All the structures showed a

good damage resistance against ballistic impacts. **Table 8** represents the residual velocity and velocity drop values for all the structures included in case 1 study. The ballistic limit velocity is found to be highest in type 3 structure (1.2 x 50 x 1.2 mm) followed by type 2 and type 1 structures. The core thickness played its role to improve the ballistic resistance of the structure. The ballistic limit velocity increased with increasing core thickness. Increase in the impact resistance of 30.6% and up to 40.8% with the increase in core thicknesses of 30 mm and 50 mm, respectively is observed. Overall, highest ballistic limit velocity and maximum damage resistance was observed in structures with 50 mm core.

Case 2 includes 1.5 mm thick face-sheet panels with all three core thicknesses. 1.5 x 20 x 1.5 mm, 1.5 x 30 x 1.5 mm , 1.5 x 50 x 1.5 mm sandwich panels configurations are included in this case and they are entitled as type 1, type 2 and type 3 respectively. Sandwich structures studied in case 2 showed better response and damage resistance than case 1 structures. Improved ballistic response was noted due to increase in face sheet thickness to 1.5 mm from 1.2 mm. Increase in the impact resistance upto 11.7% with the increase in face-sheet thicknesses of 1.5 mm is observed. Similar to case 1, highest ballistic limit velocity and maximum damage resistance was observed in structures having 50 mm core thickness. **Table 9** represents the residual velocity and velocity drop values for all the structures included in case 2 study.

Case 3 includes 2.0 mm thick face-sheet panels with all three core thicknesses. 2.0 x 20 x 2.0 mm, 2.0 x 30 x 2.0 mm , 2.0 x 50 x 2.0 mm sandwich panels configurations are included in this case and they are entitled as type 1, type 2 and type 3 respectively. Sandwich structures studied in case 3 showed overall better response and damage resistance than case 1 and case 2 structures. Improved ballistic response was observed due to increase in face sheet thickness to 2.0 mm from 1.5 mm and 1.2 mm. Increase in the impact resistance of 11.7% and up to 18.2% with the increase in face-sheet thicknesses of 1.5 mm and 2.0 mm, respectively is observed. On the other hand, increase in the impact resistance of 30.6% and up to 40.8% with the increase in core thicknesses of 30 mm and 50 mm, respectively is observed. Sandwich structures in case 3 showed high ballistic limit velocity and maximum damage resistance capabilities to impact. **Table 10** represents the residual velocity and velocity drop values for all the structures included in case 3 study.

Table 8 : Numerical Results of Sandwich Structures in Case 1.

Sandwich Structures					
1.20 x 20 x 1.20 mm Sandwich Panel					
Serial No.	**Model type**	**Configuration**	**Impact Velocity (m/s)**	**Residual Velocity (m/s)**	**Velocity Drop**
1	Type 1	1.2 x 20 x 1.2 mm	360.3	342.785	17.515
2	Type 1	1.2 x 20 x 1.2 mm	293.4	273.31	20.09
3	Type 1	1.2 x 20 x 1.2 mm	220	194.9	25.1
4	Type 1	1.2 x 20 x 1.2 mm	150	116.17	33.83
5	Type 1	1.2 x 20 x 1.2 mm	70	0	70
6	Type 1	1.2 x 20 x 1.2 mm	66.3	Ballistic limit	
1.20 x 30 x 1.20 mm Sandwich Panel					
Serial No.	Model type	Configuration	Impact Velocity (m/s)	Residual Velocity (m/s)	Velocity Drop
1	Type 2	1.2 x 30 x 1.2 mm	360.3	335.6	24.7
2	Type 2	1.2 x 30 x 1.2 mm	293.4	265.61	27.79
4	Type 2	1.2 x 30 x 1.2 mm	220	182.5	37.5
5	Type 2	1.2 x 30 x 1.2 mm	150	101.76	48.24
6	Type 2	1.2 x 30 x 1.2 mm	90	0	90
7	Type 2	1.2 x 30 x 1.2 mm	85	0	85
8	Type 2	1.2 x 30 x 1.2 mm	82.4	Ballistic limit	
1.20 x 50 x 1.20 mm Sandwich Panel					
1	Type 3	1.2 x 50 x 1.2 mm	360.3	326.51	33.79
2	Type 3	1.2 x 50 x 1.2 mm	293.4	236.82	56.58
3	Type 3	1.2 x 50 x 1.2 mm	220	159.63	60.37
4	Type 3	1.2 x 50 x 1.2 mm	150	69.35	80.65
5	Type 3	1.2 x 50 x 1.2 mm	112	0	112
6	Type 3	1.2 x 50 x 1.2 mm	107.4	Ballistic limit	

Table 9 : Numerical Results of Sandwich Structures in Case 2.

Sandwich Structures					
1.50 x 20 x 1.50 mm Sandwich Panel					
Serial No.	**Model type**	**Configuration**	**Impact Velocity (m/s)**	**Residual Velocity (m/s)**	**Velocity Drop**
1	Type 1	1.5 x 20 x 1.5 mm	360.3	341.08	19.22
2	Type 1	1.5 x 20 x 1.5 mm	293.4	270.68	22.72
3	Type 1	1.5 x 20 x 1.5 mm	220	192.11	27.89
4	Type 1	1.5 x 20 x 1.5 mm	150	112.21	37.79
5	Type 1	1.5 x 20 x 1.5 mm	85	0	85
6	Type 1	1.5 x 20 x 1.5 mm	71.6	Ballistic Limit	
1.50 x 30 x 1.50 mm Sandwich Panel					
Serial No.	**Model type**	**Configuration**	**Impact Velocity (m/s)**	**Residual Velocity (m/s)**	**Velocity Drop**
1	Type 2	1.5 x 30 x1.5 mm	360.3	332.62	27.68
2	Type 2	1.5 x 30 x 1.5 mm	293.4	263.75	29.65
4	Type 2	1.5 x 30 x 1.5 mm	220	183.21	36.75
5	Type 2	1.5 x 30 x 1.5 mm	150	100.02	49.98
6	Type 2	1.5 x 30 x 1.5 mm	85	0	85
7	Type 2	1.5 x 30 x 1.5 mm	83.5	Ballistic Limit	-
1.50 x 50 x 1.50 mm Sandwich Panel					
1	Type 3	1.5 x 50 x 1.5 mm	360.3	325.2	35.1
2	Type 3	1.5 x 50 x 1.5 mm	293.4	255.31	38.09
3	Type 3	1.5 x 50 x 1.5 mm	220	175.61	44.39

4	Type 3	1.5 x 50 x 1.5 mm	150	90.62	59.38
5	Type 3	1.5 x 50 x 1.5 mm	112	0	112
6	Type 3	1.5 x 50 x 1.5 mm	108.1	Ballistic Limit	-

Table 10 : Numerical Results of Sandwich Structures in Case 3.

Sandwich Structures					
2.0 x 20 x 2.0 mm Sandwich Panel					
Serial No.	**Model type**	**Configuration**	**Impact Velocity (m/s)**	**Residual Velocity (m/s)**	**Velocity Drop**
1	Type 1	2.0 x 20 x 2.0 mm	360.3	339.12	21.18
2	Type 1	2.0 x 20 x 2.0 mm	293.4	268.55	24.85
3	Type 1	2.0 x 20 x 2.0 mm	220	188.11	31.89
4	Type 1	2.0 x 20 x 2.0 mm	150	104.7	45.3
5	Type 1	2.0 x 20 x 2.0 mm	80	0	-
6	Type 1	2.0 x 20 x 2.0 mm	75	0	-
7	Type 1	2.0 x 20 x 2.0 mm	73.3	Ballistic limit	-
2.0 x 30 x 2.0 mm Sandwich Panel					
Serial No.	**Model type**	**Configuration**	**Impact Velocity (m/s)**	**Residual Velocity (m/s)**	**Velocity Drop**
1	Type 2	2.0 x 30 x 2.0 mm	360.3	330.51	29.79
2	Type 2	2.0 x 30 x 2.0 mm	293.4	258.85	34.55
4	Type 2	2.0 x 30 x 2.0 mm	220	177.4	42.6
5	Type 2	2.0 x 30 x 2.0 mm	150	88.89	61.11
6	Type 2	2.0 x 30 x 2.0 mm	95	0	-
7	Type 2	2.0 x 30 x 2.0 mm	92	0	-

8	Type 2	1.2 x 30 x1.2 mm	91.1	Ballistic limit	-
2.0 x 50 x 2.0 mm Sandwich Panel					
1	Type 3	2.0 x 50 x 2.0 mm	360.3	309.04	51.26
2	Type 3	2.0 x 50 x 2.0 mm	293.4	234.78	58.62
3	Type 3	2.0 x 50 x 2.0 mm	220	158.83	61.17
4	Type 3	2.0 x 50 x 2.0 mm	150	48.68	101.46
5	Type 3	2.0 x 50 x 2.0 mm	120	0	-
6	Type 3	2.0 x 50 x 2.0 mm	115	0	-
7	Type 3	2.0 x 50 x 2.0 mm	113.2	Ballistic limit	-

Residual velocity data graphs for all configurations are shown in **Figure 19, Figure 20, Figure 21.**

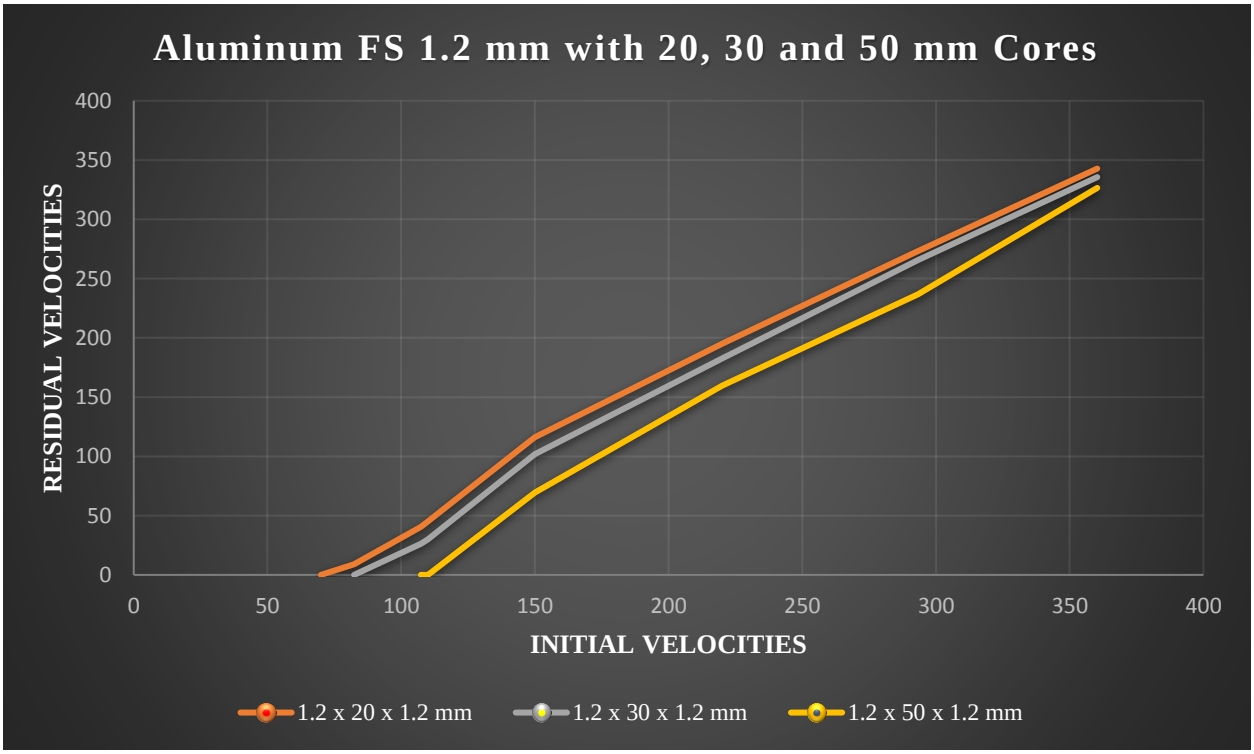

Figure 19 : Residual velocity Data for Case 1 sandwich structures

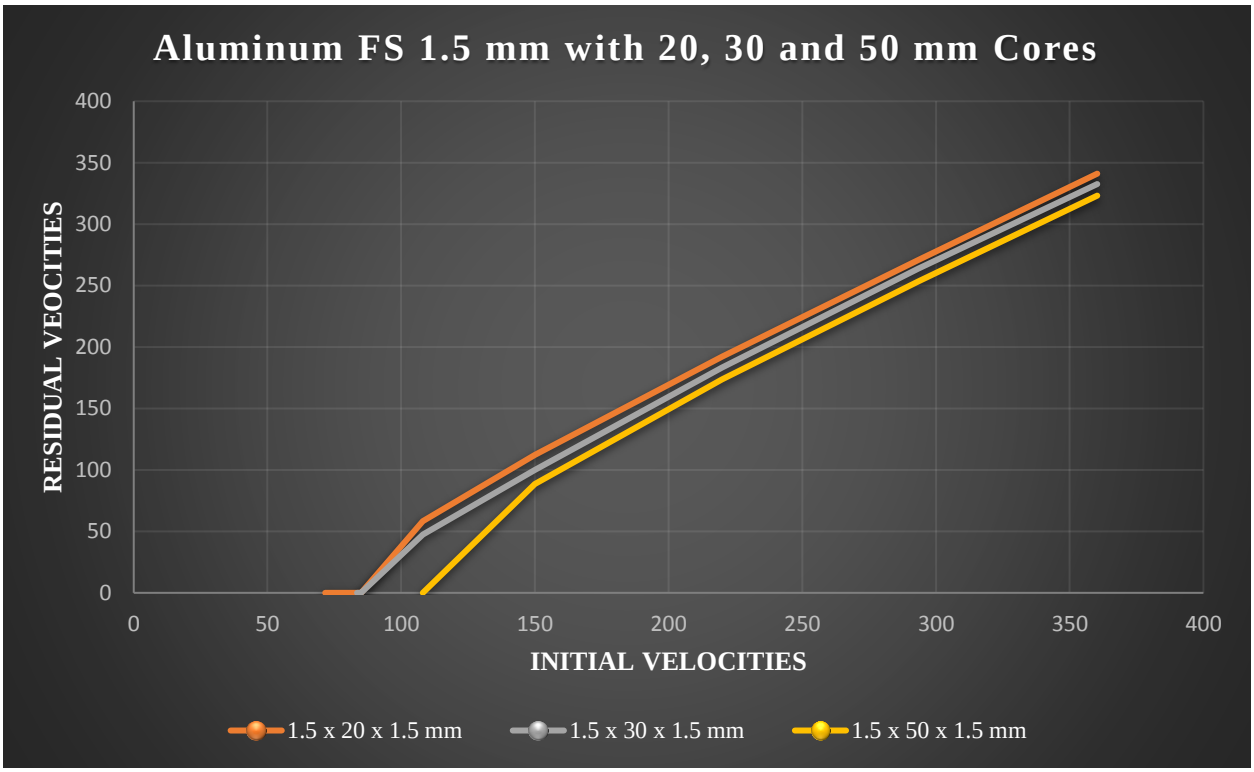

Figure 20 : Residual velocity Data for Case 2 sandwich structures

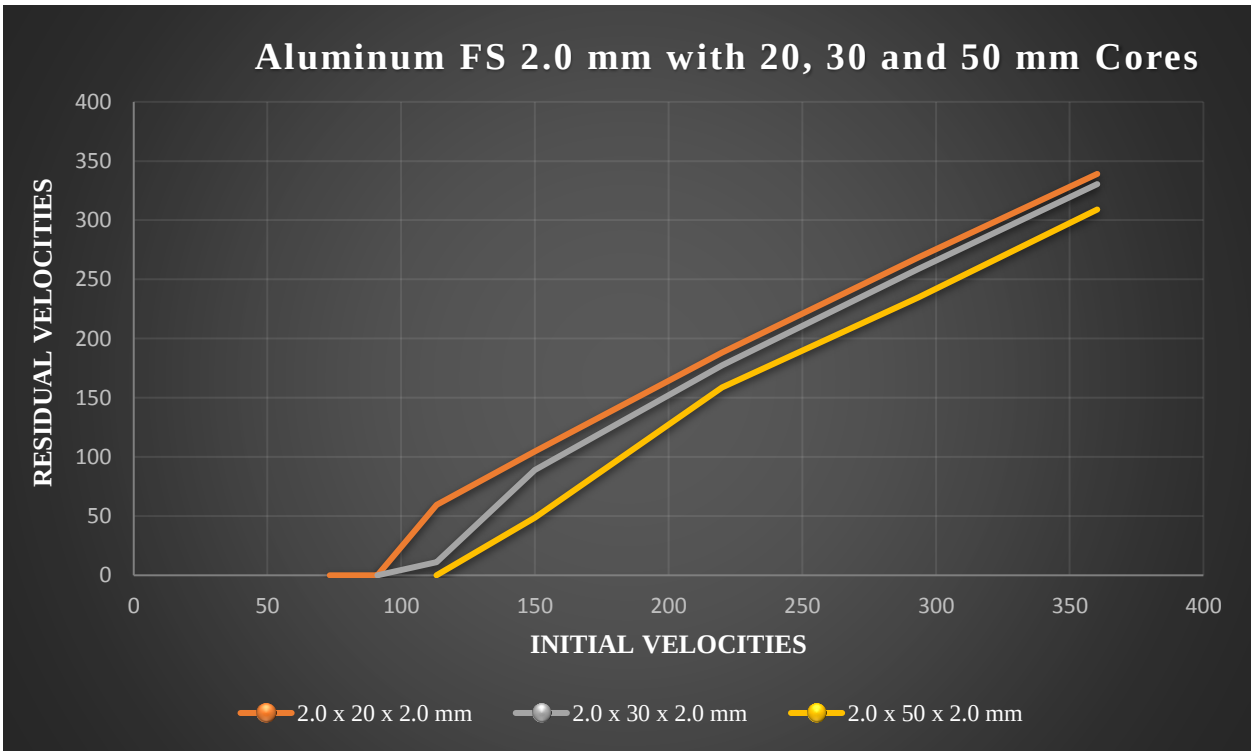

Figure 21 : Residual Velocity data for case 3 sandwich structures.

Based on results, both the materials showed ductile hole formation upon failure. Ogival nose projectiles penetrates the targets mainly by ductile, hole-growth deformation pushing the material in front of projectile aside. Petal development, which is typical in thin ductile targets, caused the face sheets to collapse. In thin targets, projectiles are responsible for Petalling causing radial cracking due to high circumferential strains and subsequent rotation of the deformed target material resulting in a number of petals. Petals were formed at front side of fully perforated face sheets at all velocities. **Figure 18** represents the petal formation in face sheets in a fully perforated structure. TPU core acted as highly ductile material and material fragmentations of TPU core appeared when impacted at high velocity. **Figure 17** shows the fragments of core material in a fully perforated structure. **Figure 22** represents the Progression of the projectile through the composite sandwich structure at various time intervals.

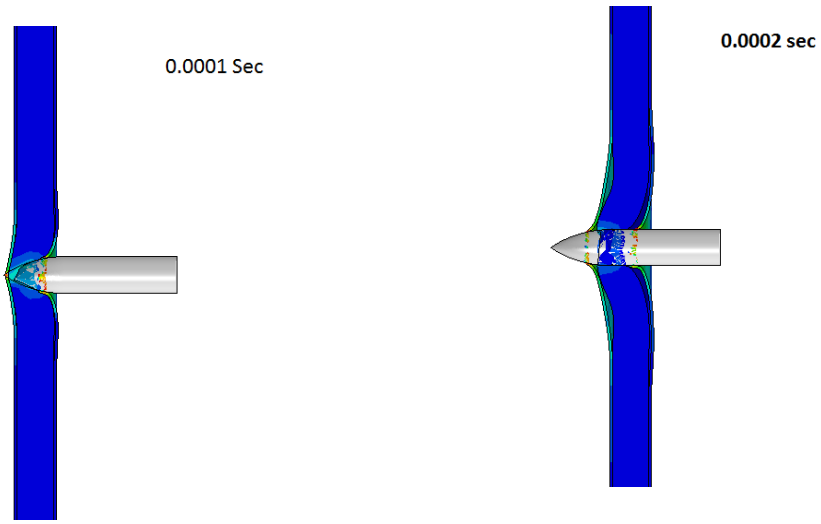

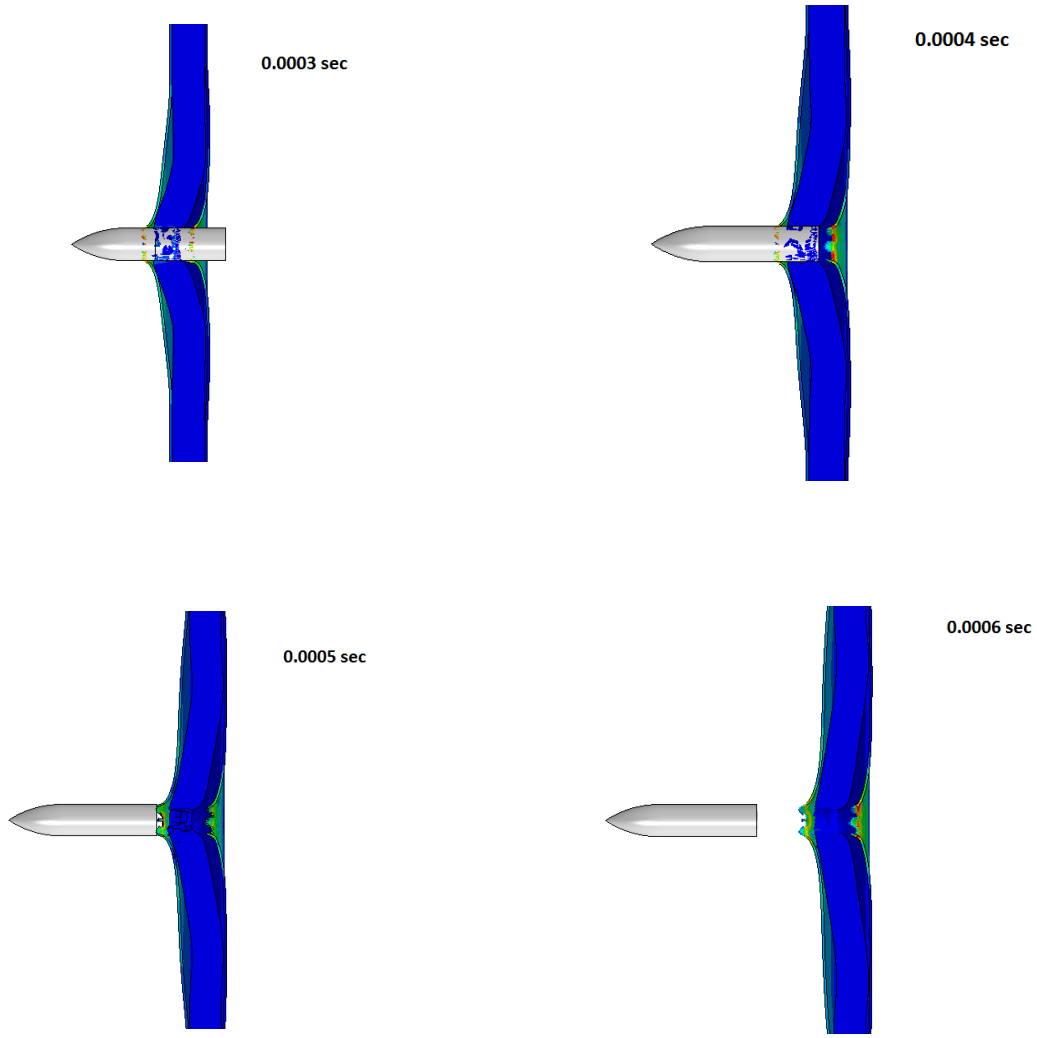

Figure 22 : Progression of the projectile through the composite sandwich structure at various time intervals.

5. Conclusions

Numerical investigation on Thermoplastic Polyurethane foam based sandwiches has been undertaken using finite element analysis package Abaqus/Explicit. The explained methodology of numerical simulations and physics of material models were proved to be efficient and reliable to characterize the impact response of composite armor structure against high speed impact. Various configurations of composite armor were numerically tested to study their response against ogival nose shape projectile.

The study reveals that the mechanics of perforation are highly sophisticated and are dependent on a number of variables. Various key factors including target configuration, material parameters, projectile nose shape and impact velocities influence the response of composite armor against high speed impact. Ballistic limit velocities were also found out for each composite armor structure. It was found to be increasing with increasing thickness of sandwich panels. The ballistic limit velocity was found out to be highest for sandwich panel of type 3 of case 3 (2.0 mm thick face skin with 50 mm core) as it offers more energy absorption and resistance to impacting projectile. It was observed that the global deformation decreases with increased impact velocity. The highest global deformation was observed at the ballistic limit velocities of sandwich structures.

Projectile shape is one of the key factor that decides the formation of hole structure in target. Ogive nose projectiles are one of the most efficient penetrator for the thin ductile targets. Projectiles with an ogival nose penetrate primarily by ductile, hole growth deformation, which pushes the material in front of the projectile aside. In thin targets, projectiles are responsible for Petalling causing radial cracking due to high circumferential strains and subsequent rotation of the deformed target material resulting in a number of petals. The failure of the face sheets in sandwich panels was caused by the formation of petals, which is common in thin ductile targets. Polymer core which is also highly ductile failed mainly due to ductile hole formation and material fragmentations of TPU were observed upon failure.

Target configuration, an influencing factor on protective performance has a strong effect on impact penetration and perforation resistance. The sandwich panels with thick core exhibit better energy absorption and impact resistance capabilities than sandwich panels with thin core. Similarly, with thin face skins, the protective performance of sandwich panel decreases due to less energy

absorption and resistance to impact. The protective performance tends to increase with increasing target thickness. At high speed impact, the diffused and localized deformation of sandwich panels tends to decrease and it increases with the increase in sandwich panel's thickness. Increasing the thickness of face sheets and Core served to increase the impact and damage resistance. Increasing the thickness of face sheets from 1.2 mm to 1.5 mm and 2 mm thicknesses can enhance the ballistic resistance of structure up to 11.7% and 18.2%, respectively. By increasing the core thickness from 20 mm to 30 mm and 50 mm , ballistic resistance can be enhanced up to 30.6% and 40.8%, respectively.

The numerical methodology is found to be more efficient and reliable in the prediction of ballistic limit velocities and damage resistance of composite armor structures with more accurate results and this surely can replace the time consuming and expensive dynamic experiments**.**

References:

[1] L. J. Gibson and M. F. Ashby, *Cellular Solids*. Cambridge University Press, 1997.

[2] S. A. Tekalur, A. E. Bogdanovich, and A. Shukla, "Shock loading response of sandwich panels with 3-D woven E-glass composite skins and stitched foam core," *Compos. Sci. Technol.*, vol. 69, no. 6, pp. 736–753, 2009, doi: 10.1016/j.compscitech.2008.03.017.

[3] K. P. Dharmasena, H. N. G. Wadley, Z. Xue, and J. W. Hutchinson, "Mechanical response of metallic honeycomb sandwich panel structures to high-intensity dynamic loading," *Int. J. Impact Eng.*, vol. 35, no. 9, pp. 1063–1074, 2008, doi: 10.1016/j.ijimpeng.2007.06.008.

[4] E. Wang, N. Gardner, and A. Shukla, "The blast resistance of sandwich composites with stepwise graded cores," *Int. J. Solids Struct.*, vol. 46, no. 18–19, pp. 3492–3502, 2009, doi: 10.1016/j.ijsolstr.2009.06.004.

[5] M. Z. Hassan, Z. W. Guan, W. J. Cantwell, G. S. Langdon, and G. N. Nurick, "The influence of core density on the blast resistance of foam-based sandwich structures," *Int. J. Impact Eng.*, vol. 50, pp. 9–16, 2012, doi: 10.1016/j.ijimpeng.2012.06.009.

[6] C. Qi, S. Yang, L. J. Yang, Z. Y. Wei, and Z. H. Lu, "Blast resistance and multi-objective optimization of aluminum foam-cored sandwich panels," *Compos. Struct.*, vol. 105, pp. 45–57, 2013, doi: 10.1016/j.compstruct.2013.04.043.

[7] Z. W. Guan, A. Aktas, P. Potluri, W. J. Cantwell, G. Langdon, and G. N. Nurick, "The blast resistance of stitched sandwich panels," *Int. J. Impact Eng.*, vol. 65, pp. 137–145, 2014, doi: 10.1016/j.ijimpeng.2013.12.001.

[8] C. C. By-nc-nd, "Wang , H ., Ramakrishnan , K . R ., & Shankar , K . (2016). Experimental study of the medium velocity impact response of sandwich panels with," pp. 68–82, 2016.

[9] A. G. Evans, "Lightweight Materials and Structures," *MRS Bull.*, vol. 26, no. 10, pp. 790–797, Oct. 2001, doi: 10.1557/mrs2001.206.

[10] D. W. Zhou and W. J. Stronge, "Ballistic limit for oblique impact of thin sandwich panels and spaced plates," *Int. J. Impact Eng.*, vol. 35, no. 11, pp. 1339–1354, 2008, doi:

10.1016/j.ijimpeng.2007.08.004.

[11] I. Marom and S. R. Bodner, “Projectile perforation of multi-layered beams,” *Int. J. Mech. Sci.*, vol. 21, no. 8, pp. 489–504, 1979, doi: 10.1016/0020-7403(79)90011-0.

[12] V. Dey, G. Zani, M. Colombo, M. Di Prisco, and B. Mobasher, “Flexural impact response of textile-reinforced aerated concrete sandwich panels,” *Mater. Des.*, vol. 86, pp. 187–197, 2015, doi: 10.1016/j.matdes.2015.07.004.

[13] J. Radin and W. Goldsmith, “Normal projectile penetration and perforation of layered targets,” *Int. J. Impact Eng.*, vol. 7, no. 2, pp. 229–259, 1988, doi: 10.1016/0734-743X(88)90028-0.

[14] S. Ryan, H. Li, M. Edgerton, D. Gallardy, and S. J. Cimpoeru, “The ballistic performance of an ultra-high hardness armour steel: An experimental investigation,” *Int. J. Impact Eng.*, vol. 94, pp. 60–73, 2016, doi: 10.1016/j.ijimpeng.2016.03.011.

[15] T. Børvik, M. J. Forrestal, and T. L. Warren, “Perforation of 5083-H116 Aluminum Armor Plates with Ogive-Nose Rods and 7.62 mm APM2 Bullets,” *Exp. Mech.*, vol. 50, no. 7, pp. 969–978, 2010, doi: 10.1007/s11340-009-9262-5.

[16] “Abaqus 6.11**有限元分析从入**门到精通.”

[17] Livermore Software Technology Corporation, *L{S}-{DYNA} - {K}eyword {U}ser’s {M}anual, Version 970*, vol. I, no. May. 2003.

[18] R. Guide, “MSC.Dytran 2005 ®,” 2005.

[19] S. P. H. U. Manual, “AUTODYN ® Explicit Software for Nonlinear Dynamics SPH User Manual & Tutorial,” *ANSYS Inc*, 2005.

[20] T. Børvik, M. Langseth, O. S. Hopperstad, and K. A. Malo, *Ballistic penetration of steel plates*, vol. 22, no. 9. 1999.

[21] T. Borvik, O. S. Hopperstad, T. Berstad, and M. Langseth, “Perforation of 12mm thick steel plates by 20mm diameter projectiles with flat, hemispherical and conical noses - Part II: Numerical simulations,” *Int. J. Impact Eng.*, vol. 27, no. 1, pp. 37–64, 2001, doi:

10.1016/S0734-743X(01)00035-5.

[22] X. Teng, T. Wierzbicki, and M. Huang, “Ballistic resistance of double-layered armor plates,” *Int. J. Impact Eng.*, vol. 35, no. 8, pp. 870–884, 2008, doi: 10.1016/j.ijimpeng.2008.01.008.

[23] S. Dey, T. Børvik, X. Teng, T. Wierzbicki, and O. S. Hopperstad, “On the ballistic resistance of double-layered steel plates: An experimental and numerical investigation,” *Int. J. Solids Struct.*, vol. 44, no. 20, pp. 6701–6723, 2007, doi: 10.1016/j.ijsolstr.2007.03.005.

[24] T. Børvik, S. Dey, and A. H. Clausen, “Perforation resistance of five different high-strength steel plates subjected to small-arms projectiles,” *Int. J. Impact Eng.*, vol. 36, no. 7, pp. 948–964, 2009, doi: 10.1016/j.ijimpeng.2008.12.003.

[25] N. Kiliç and B. Ekici, “Ballistic resistance of high hardness armor steels against 7.62 mm armor piercing ammunition,” *Mater. Des.*, vol. 44, no. February, pp. 35–48, 2013, doi: 10.1016/j.matdes.2012.07.045.

[26] V. Paris, A. Weiss, A. Vizel, E. Ran, and F. Aizik, “Fragmentation of armor piercing steel projectiles upon oblique perforation of steel plates,” *EPJ Web Conf.*, vol. 26, pp. 1–6, 2012, doi: 10.1051/epjconf/20122604032.

[27] N. Kılıç, B. Ekici, and S. Bedir, “Optimization of high hardness perforated steel armor plates using finite element and response surface methods,” *Mech. Adv. Mater. Struct.*, vol. 24, no. 7, pp. 615–624, 2017, doi: 10.1080/15376494.2016.1196771.

[28] M. J. Pawar *et al.*, “Comparison of ballistic performances of Al2O3 and AlN ceramics,” *Int. J. Impact Eng.*, vol. 98, pp. 42–51, 2016, doi: 10.1016/j.ijimpeng.2016.08.002.

[29] Z. Rosenberg, R. Kositski, and E. Dekel, “On the perforation of aluminum plates by 7.62 mm APM2 projectiles,” *Int. J. Impact Eng.*, vol. 97, pp. 79–86, 2016, doi: 10.1016/j.ijimpeng.2016.06.003.

[30] N. Kiliç and B. Ekici, “Ballistic resistance of high hardness armor steels against 7.62 mm armor piercing ammunition,” *Mater. Des.*, vol. 44, pp. 35–48, 2013, doi: 10.1016/j.matdes.2012.07.045.

[31] D. E. Tria and R. Trębiński, “Methodology for experimental verification of steel armour impact modelling,” *Int. J. Impact Eng.*, vol. 100, pp. 102–116, 2017, doi: 10.1016/j.ijimpeng.2016.10.011.

[32] A. Jamil, Z. W. Guan, and W. J. Cantwell, “The static and dynamic response of CFRP tube reinforced polyurethane,” *Compos. Struct.*, vol. 161, pp. 85–92, 2017, doi: 10.1016/j.compstruct.2016.11.043.

[33] A. Jamil, Z. W. Guan, W. J. Cantwell, X. F. Zhang, G. S. Langdon, and Q. Y. Wang, “Blast response of aluminium/thermoplastic polyurethane sandwich panels – experimental work and numerical analysis,” *Int. J. Impact Eng.*, vol. 127, no. January, pp. 31–40, 2019, doi: 10.1016/j.ijimpeng.2019.01.003.

[34] “Stress-Strain Curve: Strength of Materials | SMLease Design.” https://www.smlease.com/entries/mechanical-design-basics/stress-strain-curve-diagram/ (accessed Sep. 06, 2021).

[35] “Exploring the Stress / Strain Curve for Mild Steel - The Chicago Curve.” https://www.cmrp.com/blog/faq/analysis-design/exploring-stress-strain-curve-mild-steel.html (accessed Sep. 06, 2021).

[36] A. Mansur, *Modeling of Mechanical Properties of Ceramic-Metal Composites for Armor Applications*, no. February. 2011.

[37] T. Borvik, O. S. Hopperstad, T. Berstad, and M. Langseth, “A computational model of viscoplasticity and ductile damage for impact and penetration,” *Eur. J. Mech. A/Solids*, vol. 20, no. 5, pp. 685–712, 2001, doi: 10.1016/S0997-7538(01)01157-3.

[38] M. M. Nazeer, M. A. Khan, A. Naeem, and A. U. Haq, “Analysis of conical tool perforation of ductile metal sheets,” *Int. J. Mech. Sci.*, vol. 42, no. 7, pp. 1391–1403, 2000, doi: 10.1016/S0020-7403(99)00065-X.

[39] A. Rusinek, J. A. Rodríguez-Martínez, R. Zaera, J. R. Klepaczko, A. Arias, and C. Sauvelet, “Experimental and numerical study on the perforation process of mild steel sheets subjected to perpendicular impact by hemispherical projectiles,” *Int. J. Impact Eng.*, vol. 36, no. 4, pp. 565–587, 2009, doi: 10.1016/j.ijimpeng.2008.09.004.

[40] B. Wang, G. Lu, and M. K. Lim, “Experimental and numerical analysis of the response of aluminium oxide tiles to impact loading,” *J. Mater. Process. Tech.*, vol. 51, no. 1–4, pp. 321–345, 1995, doi: 10.1016/0924-0136(94)01604-Y.

[41] J. G. Hetherington and P. F. Lemieux, “The effect of obliquity on the ballistic performance of two component composite armours,” *Int. J. Impact Eng.*, vol. 15, no. 2, pp. 131–137, 1994, doi: 10.1016/S0734-743X(05)80026-0.

[42] “Corti~s, c. navarro,” *Young*, vol. 12, no. 4, pp. 639–650, 1992.

[43] S. Sadanandan and J. G. Hetherington, “Characterisation of ceramic/steel and ceramic/aluminium armours subjected to oblique impact,” *Int. J. Impact Eng.*, vol. 19, no. 9–10, pp. 811–819, 1997, doi: 10.1016/s0734-743x(97)00019-5.

[44] V. B. C. Tan, V. P. W. Shim, and T. E. Tay, “Experimental and numerical study of the response of flexible laminates to impact loading,” *Int. J. Solids Struct.*, vol. 40, no. 23, pp. 6245–6266, 2003, doi: 10.1016/S0020-7683(03)00413-X.

[45] A. H. Sheikh, P. H. Bull, and J. A. Kepler, “Behaviour of multiple composite plates subjected to ballistic impact,” *Compos. Sci. Technol.*, vol. 69, no. 6, pp. 704–710, 2009, doi: 10.1016/j.compscitech.2008.03.022.

[46] L. J. Deka, S. D. Bartus, and U. K. Vaidya, “Multi-site impact response of S2-glass/epoxy composite laminates,” *Compos. Sci. Technol.*, vol. 69, no. 6, pp. 725–735, 2009, doi: 10.1016/j.compscitech.2008.03.002.

[47] M. A. G. Silva, C. Cismaşiu, and C. G. Chiorean, “Numerical simulation of ballistic impact on composite laminates,” *Int. J. Impact Eng.*, vol. 31, no. 3, pp. 289–306, 2005, doi: 10.1016/j.ijimpeng.2004.01.011.

[48] A. Morka and J. Nowak, “Numerical Analyses of Ceramic/Metal Ballistic Panels Subjected To Projectile Impact,” *J. KONES. Powertrain Transp.*, vol. 19, no. 4, pp. 465–472, 2015, doi: 10.5604/12314005.1138618.

[49] H. D. Espinosa, S. Dwivedi, P. D. Zavattieri, and G. Yuan, “A numerical investigation of penetration in multilayered material/structure systems,” *Int. J. Solids Struct.*, vol. 35, no. 22, pp. 2975–3001, 1998, doi: 10.1016/S0020-7683(97)60353-4.

[50] R. Mark, A. S. Cakmak, K. Hill, and R. Davidson, “Transactions on the Built Environment vol 3, © 1993 WIT Press, www.witpress.com, ISSN 1743-3509,” vol. 3, 1993.

[51] C. Swaroop, A. K. Srivastave, and K. N. Pandey, “SPH Simulation of Ballistic Impact on Ceramic Plate,” no. 1, pp. 84–88, 2013.

[52] G. R. Johnson and W. H. Cook, “A Computational Constitutive Model and Data for Metals Subjected to Large Strain, High Strain Rates and High Pressures,” *Seventh Int. Symp. Ballist.*, pp. 541–547, 1983.

[53] ABAQUS, “Abaqus 6.14,” *Abaqus 6.14 Anal. User’s Guid.*, p. 14, 2014.

[54] N. K. Gupta, M. A. Iqbal, and G. S. Sekhon, “Effect of projectile nose shape, impact velocity and target thickness on deformation behavior of aluminum plates,” *Int. J. Solids Struct.*, vol. 44, no. 10, pp. 3411–3439, 2007, doi: 10.1016/j.ijsolstr.2006.09.034.

[55] NATO, “Procedures for Evaluating the Protection Level of Armoured Vehicles - Ied Threat,” *Aep-55-Vol-3*, p. 106, 2008.

[56] T. Børvik, M. J. Forrestal, O. S. Hopperstad, T. L. Warren, and M. Langseth, “Perforation of AA5083-H116 aluminium plates with conical-nose steel projectiles - Calculations,” *Int. J. Impact Eng.*, vol. 36, no. 3, pp. 426–437, 2009, doi: 10.1016/j.ijimpeng.2008.02.004.

[57] A. H. Clausen, T. Børvik, O. S. Hopperstad, and A. Benallal, “Flow and fracture characteristics of aluminium alloy AA5083-H116 as function of strain rate, temperature and triaxiality,” *Mater. Sci. Eng. A*, vol. 364, no. 1–2, pp. 260–272, 2004, doi: 10.1016/j.msea.2003.08.027.

[58] D. R. Scheffler, “Modeling the Effect of Penetrator Nose Shape on Threshold Velocity for Thick Aluminum Targets,” no. July, 1997.

[59] M. A. Iqbal, A. Chakrabarti, S. Beniwal, and N. K. Gupta, “3D numerical simulations of sharp nosed projectile impact on ductile targets,” *Int. J. Impact Eng.*, vol. 37, no. 2, pp. 185–195, 2010, doi: 10.1016/j.ijimpeng.2009.09.008.

[60] H. M. Wen, T. Y. Reddy, S. R. Reid, and P. D. Soden, “Indentation, penetration and

perforation of composite laminates and sandwich panels under quasi-static and projectile loading," *Key Eng. Mater.*, no. 143 PART II, pp. 501–552, 1998, doi: 10.4028/www.scientific.net/kem.141-143.501.

[61] Z. Rosenberg and E. Dekel, *Terminal ballistics*. 2020.